

CORROSION BEHAVIOUR OF NANOSTRUCTURED ALUMINIUM ALLOYS PROCESSED BY CRYO-ROLLING

A DISSERTATION

*Submitted in partial fulfillment of the
requirements for the award of the degree*

of

MASTER OF TECHNOLOGY

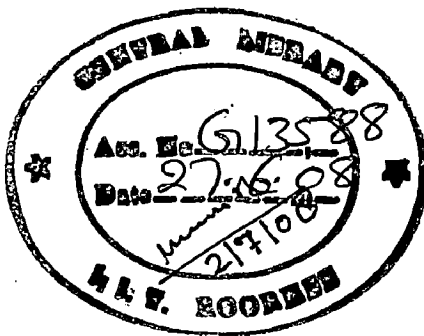
in

METALLURGICAL & MATERIALS ENGINEERING

(With Specialization in Corrosion Engineering)

By

SANJEEV KUMAR



DEPARTMENT OF METALLURGICAL & MATERIALS ENGINEERING
INDIAN INSTITUTE OF TECHNOLOGY ROORKEE

ROORKEE -247 667 (INDIA)

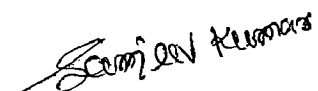
JUNE, 2007

CANDIDATE'S DECLARATION

This is to certify that the dissertation work which is being presented here titled "**Corrosion behavior of nanostructured aluminium alloys processed by cryo-rolling**" in partial fulfillment of the requirement for the award of degree of **Master of Technology in Metallurgical and Materials Engineering** with specialization in **Corrosion Engineering**, submitted in the **Department of Metallurgical and Materials Engineering, Indian Institute of Technology Roorkee**, is an authentic record of my own work carried out during the period from May 2006 to June 2007 under the guidance of **Dr. R. Jayaganthan**, Assistant Professor, Department of Metallurgical and Materials Engineering, Indian Institute of Technology Roorkee.

The matter embodied in this dissertation has not been submitted for award of any other degree or diploma.

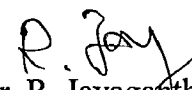
Dated: June 30, 2007


(Sanjeev Kumar)
En. No. 7055504

CERTIFICATE

This is to certify that above declaration by Mr. Sanjeev Kumar is true to best of my knowledge.

Dated: June 30, 2007


(Dr. R. Jayaganthan)

Assistant Professor

Dept. of Metallurgical and Materials Engineering

Indian Institute of Technology Roorkee

Roorkee-247667

India

ACKNOWLEDGEMENTS

I express deep gratitude to my guide **Dr. R. Jayagathan**, Associate Professor, Department of Metallurgical and Materials Engineering Department, Indian Institute of Technology Roorkee, for his inspiration and active supervision, through provoking discussing criticism and suggestion given by him during the course of this work. He gave invaluable guidance and motivation at each and every step of my work without which this work would have been inconceivable. He was always with me whenever required with his useful suggestions and being patient with me through all the time. I am really very grateful to him for his cares shown towards me. It was an honour and great pleasure for me to work with him.

I am extremely grateful to **Dr. S.K. Nath**, Professor and Head of the Department, Department of Metallurgical and Materials Engineering, Indian Institute of Technology Roorkee, for providing me all the facilities in the department to carry out my dissertation work.

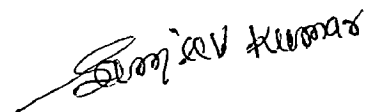
I would also like to express my gratitude to **Dr. Devendra Puri**, O.C. M. Tech. and Assistant Professor and **S. Ray**, Professor Department of Metallurgical and Materials Engineering, Indian Institute of Technology Roorkee for providing me opportunity to present this dissertation work.

It is hard to express my feeling in proper words for my parents who apart from providing me the best available education. They have always encouraged me in all endeavors. I owe much of my academic success to them.

I am thankful to technical staff of Department Metallurgical and Materials Engineering, Indian Institute of Technology Roorkee.

Lastly, though it is not possible to mention every one, none can be forgotten for their direct and indirect help.

Dated: June 30, 2007


(SANJEEV KUMAR)

ABSTRACT

The present work is envisaged to study the corrosion behavior of ultrafine grained aluminium alloys processed by cryo-rolling. The chemical compositions of this alloy by weight % are 0.45% Si, 0.3% Mg, 0.05%Cu, 0.013% Mn, 0.048 %Fe, 0.22% Zn, 0.022% Cr and the remaining are aluminium in wet environments. Five different thickness of cryo-rolled aluminium alloy samples of three sets each were subjected to salt spray corrosion tests (ASTM-B117 standard) for 24 hours, 48 hours, and 72 hours respectively. Three different thickness of cryo-rolled aluminium alloys were also subjected to immersion tests. The weight loss kinetics curves of the alloys, in 3.5% NaCl environment, were measured. The surface morphology of the corroded alloys was characterized by FE-SEM. Upon exposed to the corrosive environment, a localized type of attack occurs on the samples and showed the presence of Al_2O_3 , MgO , ZnO , Cr_2O_3 , Cu_2O , Fe_2O_3 , Na_2O , SiO_2 . However, the dominant phase was aluminium oxide for all thickness samples. From the surface morphology of the corroded samples, we found that a less thickness sample undergo corrosion at a relatively faster rate when compared to larger thickness sample.

TABLE OF CONTENTS

	Page no.
Candidates's Declaration.....	i
Acknowledgements.....	ii
Abstract.....	iii
List of Figures.....	v
List of Tables.....	vii
Chapter	
1. Introduction.....	1
2. Literature Survey.....	4
2.1 Introduction.....	4
2.2 Effect of cryo-rolling on corrosion behavior.....	8
2.3 Metallurgical tempers of high-strength alloys.....	9
2.4 Corrosion behavior.....	9
2.5 Corrosion inhibition of aluminium alloys by rare earth chlorides..	11
3. Formulation of the Problem.....	13
4. Experimental Procedure.....	15
4.1 Materials formulation.....	15
4.2 Sample preparation.....	15
4.3 Salt spray machine.....	16
4.4 salt spray corrosion tests.....	16
4.5 Sources of error.....	17
4.6 Precautions.....	17
4.7 Salt immersion tests.....	18
5. Results and Discussions.....	19
5.1. Visual observation.....	19
5.2. Thermo gravimetric analysis.....	20
5.3 X-ray Diffraction Analysis.....	22
5.4 FESEM Results.....	33
5.5 Discussions.....	39
6. Conclusions.....	40
7. Suggestions for Future work.....	41
References.....	42

List of figures

Number	Description	Page
2.1	Pourbaix diagram for aluminium with $\text{Al}_2\text{O}_3 \cdot 3\text{H}_2\text{O}$ film at 25°C. Potential values are for the standard hydrogen electrode (SHE) scale.....	10
2.2	Corrosion behavior under different environment.....	10
5.1	XRD pattern for 24 hours salt spray test for specimen thickness t_1	25
5.2	XRD pattern for 24 hours salt spray test for specimen thickness t_2	25
5.3	XRD pattern for 24 hours salt spray test for specimen thickness t_3	26
5.4	XRD pattern for 24 hours salt spray test for specimen thickness t_4	26
5.5	XRD pattern for 24 hours salt spray test for specimen thickness t_5	27
5.6	XRD pattern for 48 hours salt spray test for specimen thickness t_1	27
5.7	XRD pattern for 48 hours salt spray test for specimen thickness t_2	28
5.8	XRD pattern for 48 hours salt spray test for specimen thickness t_3	28
5.9	XRD pattern for 48 hours salt spray test for specimen thickness t_4	29
5.10	XRD pattern for 48 hours salt spray test for specimen thickness t_5	29
5.11	XRD pattern for 72 hours salt spray test for specimen thickness t_1	30
5.12	XRD pattern for 72 hours salt spray test for specimen thickness t_2	30
5.13	XRD pattern for 72 hours salt spray test for specimen thickness t_3	31
5.14	XRD pattern for 72 hours salt spray test for specimen thickness t_4	31
5.15	XRD pattern for 72 hours salt spray test for specimen thickness t_5	32

5.16	EDAX pattern and its SEM image of specimen of thickness t_1 undergo 24 hours salt spray test.....	33
5.17	EDAX pattern and its SEM image of specimen of thickness t_2 undergo 24 hours salt spray test.....	33
5.18	EDAX pattern and its SEM image of specimen of thickness t_3 undergo 24 hours salt spray test.....	34
5.19	EDAX pattern and its SEM image of specimen of thickness t_4 undergo 24 hours salt spray test.....	34
5.20	EDAX pattern and its SEM image of specimen of thickness t_5 undergo 24 hours salt spray test.....	34
5.21	EDAX pattern and its SEM image of specimen of thickness t_1 undergo 48 hours salt spray test.....	35
5.22	EDAX pattern and its SEM image of specimen of thickness t_2 undergo 48 hours salt spray test.....	35
5.23	EDAX pattern and its SEM image of specimen of thickness t_3 undergo 48 hours salt spray test.....	35
5.24	EDAX pattern and its SEM image of specimen of thickness t_4 undergo 48 hours salt spray test.....	36
5.25	EDAX pattern and its SEM image of specimen of thickness t_5 undergo 48 hours salt spray test.....	36
5.26	EDAX pattern and its SEM image of specimen of thickness t_1 undergo 72 hours salt spray test.....	37
5.27	EDAX pattern and its SEM image of specimen of thickness t_2 undergo 72 hours salt spray test.....	37
5.28	EDAX pattern and its SEM image of specimen of thickness t_3 undergo 72 hours salt spray test.....	37
5.29	EDAX pattern and its SEM image of specimen of thickness t_4 undergo 72 hours salt spray test.....	38
5.30	EDAX pattern and its SEM image of specimen of thickness t_5 undergo 72 hours salt spray test.....	38

LIST OF TABLES

Number	Description	Page
4.1	Nominal composition by Wt. % of Cr-Al-alloys.....	15
4.2	Maximum Allowable Limits for Impurity Levels in NaCl.....	16
5.1	Thermo gravimetric data for immersion test.....	20
5.2	Thermo gravimetric data for salt spray test for 24 hours.....	21
5.3	Thermo gravimetric data for salt spray test for 48 hours.....	21
5.4	Thermo gravimetric data for salt spray test for 72 hours.....	22

During recent years, a lot of interest has been shown in the production of materials with nano-sized grains, especially in bulk materials through a severe plastic deformation (SPD). This interest is due to unique physical and mechanical properties inherent to various nano structured materials (NSM), e.g., processed by gas condensation or ball milling with subsequent consolidation. Besides, several specific advantages of SPD processed materials are found as compared to other NSM. In particular, SPD methods overcome number of difficulties connected with residual porosity in compacted samples, impurities from ball milling, processing of large-scale billets and engineering application of given materials [1–8]. Formation of nanostructures can be realized by SPD methods, which provides very large deformations at relatively low temperatures under high pressures [1–3]. Special methods of mechanical deformation such as equal channel angular pressing, accumulative roll bonding, multiple compression, etc., were developed to fabricate bulk nanostructured or ultra fine grain (UFG) samples and billets [4–8] out of different metals and alloys including a number of commercial alloys and intermetallics. However, majority of these methods require large plastic deformations (strains much larger than unity), complicated procedures because of which it is difficult to produce continuously long length products. On the other hand, rolling of pure copper at cryogenic temperature [9] resulted in ultra fine grains at lower plastic deformation when compared to other SPD processes at ambient or elevated temperatures. Similarly, the application of cryo-rolling to commercially pure Al is anticipated to result in UFG structure, with less plastic deformation than other SPD processes. Recent investigations of UFG metals mainly concentrated on the structural characterization [10–12], thermal stability [10], elastic and damping properties [13], micro hardness [14], compression and tensile behavior [12] and fatigue [15]. On the other hand, the corrosion behaviors of nanostructured and ultrafine grained materials have received only limited attention. A thorough knowledge of corrosion behavior of the UFG materials is important for engineering applications and also for understanding the corrosion mechanism. Corrosion in polycrystalline materials is largely associated with interfaces and is sensitive to the grain boundary structure. Therefore, the corrosion studies on UFG materials are expected

to throw some light on the specific role of grain boundaries in nanocrystalline materials. In the present work, cryo-rolling was carried out on aluminium alloys having chemical composition by weight % are 0.45% Si, 0.3% Mg, 0.05%Cu, 0.013% Mn, 0.048 %Fe, 0.22% Zn, 0.022% Cr and the remaining is aluminium to study the influence of cryogenic rolling on the corrosion behavior of aluminium alloys. In general, pitting is not regarded as a particularly damaging form of corrosion in aluminium, but it could act as a prerequisite to more severe modes of corrosion, such as stress corrosion cracking and corrosion fatigue, as they frequently initiate and grow from pits [16]. It is well known that the materials exhibit unique physical and mechanical properties when their grain size is reduced to nanometers (1–100 nm) or sub-micrometers (100–1000 nm) range. The corrosion behaviour of nanocrystalline (nc) and microcrystalline materials are expected to be different from that of the bulk polycrystalline materials due to a large difference of their grain sizes and structures. Therefore, it is very essential to investigate the corrosion behavior of nano-materials to find out if there is an improvement in their resistance corrosion or not as compared to bulk materials. Recently, the corrosion behavior of nanostructured Fe-Al-alloys studied by Zeiger et al. [17] has shown the enhancement of corrosion resistance of nanocrystalline (nc) Fe– 8 wt.% Al in Na₂SO₄ solution (pH = 6). Wang and Li [18] also reported an improved corrosion resistance of nc surface of 304 stainless steel obtained by sandblasting and annealing process in 3.5% NaCl solution. Both of them attributed the enhanced corrosion resistance to the fast diffusion of passive elements to the higher volume fraction of grain boundaries of nc materials which favored a rapid formation of the protective film. Thorpe et al. [19] found that the corrosion resistance of nc Fe₃₂Ni₃₆Cr₁₄P₁₂B₆ was greater than that of its amorphous counterpart. The authors attributed this improved corrosion resistance to the observed greater Cr-enrichment of the electrochemical surface film via rapid interphase boundary diffusion. However, Barbucci et al. [20] compared the corrosion behaviors of nanostructured Cu₉₀Ni₁₀ alloys with the coarse grained counterpart in neutral chloride solution and found a deterioration of protective properties of the oxide film on the nanostructured alloy. The authors proposed that the increased amount of grain-boundary in the nano-structured alloy and the presence of sintering defects are responsible for such a behavior. The former could justify the loss of compactness of the oxide film and the latter could prevent

regular oxide growth. Li et al. [21] found that the corrosion rate of low carbon steel in 0.05 M H₂SO₄ + 0.05 M Na₂SO₄ aqueous solution increased after being surface nano crystallized (SNC) by using ultrasonic shot peening. The corrosion rate of SNC low carbon steel decreased with the increment of grain size when the grain size was below 35 nm. The rise of the corrosion rate was attributed to having more active atoms in the grain boundary caused by SNC. Some knowledge about the corrosion performance of pure nc metals is also available. Rofagha et al. [22] investigated the corrosion behaviour of nc nickel in sulphuric acidic media. They found that the corrosion potential of nc nickel shifted about 200 mV more positively than that of polycrystalline nickel. However, nanocrystalline processing of nickel catalyzes hydrogen reduction process, reduces the kinetics of passivation, and compromises passive film stability. Youssef et al. [23] also reported improved corrosion behaviour of nanocrystalline zinc produced by pulse-current electro deposition in 0.5 mol/l NaOH solution. Aluminium, as well as its alloys, has been extensively applied in industry because of its particular properties such as low density, good appearance and corrosion resistance. For these reasons, studies on the corrosion behaviour of aluminium and its alloys are numerous. It is well known that a serious pitting corrosion will occur when aluminium and its alloys are used in an aggressive environment such as an aqueous solution containing Cl⁻. Thus, it will be interesting to see how nano-crystallization or micro-crystallization influences the corrosion behaviour of aluminium. The pitting corrosion resistance of Al alloys when the grain size is reduced to nanometers or sub-micron is not reported in the literature so far. Also, the general corrosion behavior of ultrafine grained Al alloys is scanty in the literature. Therefore, the present work has been focused to study the corrosion behavior of ultrafine grained Al alloys produced, by cryo-rolling, using salt spray and immersion techniques.

2.1 Introduction

Aluminium does not have good casting or mechanical properties. These properties can be achieved by adding magnesium and silicon to aluminium. The addition of these alloying elements increases the aluminium response to heat treatment due to formation of Mg_2Si intermetallic compound, which improves the casting, corrosion resistance property as well as the strength of the alloy. This alloy is named as the 6063 aluminium alloy. Al-Mg-Si alloy is also known as architectural and decorative alloy; because of its easy extrudability property, distinctly superior finishing quality and strength. Almost half of all the aluminium extrusions produced in UK are used in building as reported by Helby [1]. Zajac et al. [2] in 1993 investigated the hot deformation behavior of AA 6063 and AA 6005 aluminium alloy. It was found that small amount of manganese significantly helps in homogenizing and transforming the plate like β -AlFeSi phase to more rounded α -AlFeSi phase, which increases the ductility of the material. The addition of manganese also increases quench sensitivity of the alloy even when the cooling rate is as low as $50^\circ C \text{ min}^{-1}$. This was confirmed by Musulin and Celliers [3]. They found that addition of manganese accelerates the transformation of β -AlFeSi phase to a favorable α -AlFeSi phase. Okorafor [4] investigated the corrosion resistance property of 6063 alloy in under-aged, peak-aged and over-aged conditions. The results show that weight loss and rate of weight loss were both function of exposure time and heat treatment temperature. Jiang et al. [5] found that fatigue crack propagation in crystalline material is normally divided into two successive stages. In stage I, crack develops along the active slip plane and it is normal to the direction of applied stress. In stage II, the propagation of the crack begins in under-aged 6063 Al-Mg-Si alloy. The alloy exhibits heterogeneous deformation and slip bands are formed only by one slip system. There is strong tendency for single slip system activation, which can be attributed to the high volume fraction and small size of GP zone and low content of dispersoids.

Most of this article reviews some aspect of the passivity and pitting of Al and Al-alloys. It has been suggested that anodic oxide films might control the corrosion resistance of the base metal. It is known that different factors influence the pitting of other metals and alloys the same way as that of aluminum and aluminum alloys and that the existing hypothesis of pitting mechanisms in halogen environments apply to other metals and alloys as well. Recently, the interest in localized corrosion and inhibition of Al-alloys has been revived intensely because of aging of Al-alloys which are used extensively in the aerospace industry because of increasing use of Al-alloys in the automotive industry. Four stages of pitting corrosion can be distinguished: (1) processes occurring on the passive film, at the boundary of the passive film and the solution; (2) processes occurring within the passive film, when no visible microscopic changes occur in a film; (3) formation of so-called metastable pits which initiate and grow for a short period of time below the critical pitting potential and then repassivate (this is an intermediate step in pitting); and (4) stable pit growth, above a certain potential termed the critical pitting potential. A vast number of papers have been published through the years on the growth of stable pits. Metastable pits were first described qualitatively about 30 years ago, but quantitative studies were not reported until the 1980s [1]. Concerning the first two stages the processes which lead to the breakdown of the film, hence the interaction of Cl⁻ with an oxide film-little is known. These stages are certainly dependent upon the composition and structure of the oxide film. The structural characteristics of the oxide depend on the material composition, the presence and distribution of micro-defects (vacancies, voids, etc.) as well as macro-defects (inclusions, second phase particles its size and shape), crystal structure and the degree of noncrystallinity of the oxide. Its also depends on the electrolyte composition, potential and temperature. In neutral (roughly between pH 4-9) noncomplexing solutions, the oxide film on aluminum has very low solubility. Its electronic conductivity is also very low; hence the redox reactions are blocked. However, a small current is measured during metal polarization as a result of the presence of defects in the oxide film.

The air-bourne oxide on the Al was observed to be amorphous, whereas, the structure of the oxide obtained by thermal oxidation of Al was strongly dependent on the temperature. Anodic films that were grown in a borate and tartaric acid solution on the Al

are thin, dense, coherent and amorphous, whereas films grown in sulfuric and phosphoric acids contain layers which are thick, porous and crystalline. Hence, the structure of the oxide film on aluminum can be different resulting in different chemical and physical properties. Vijn [2] has shown that the corrosion potentials of Cu, Ni, Sn, Pb, Fe, Al and Zn in chloride solutions can be related to the estimated band gap values of the corrosion reaction films most likely to be formed. Highly insulating films tend to be associated with more cathodic potentials; a fact which has been qualitatively explained in terms of electron-hole participation in the partial reactions proceeding on the film covered electrode during open-circuit corrosion. The oxide films grown in aqueous environments on the majority of metals and alloys display semi conductive properties. There are many papers studying the semi conductive properties of iron and steels but only few papers exist that deal with electronic properties of aluminum passive film. The semi conductive properties of passive films were observed to vary with environmental and material variables. For example, depending upon the heat treatment, the passive films on stainless steels exhibited either p- or n-type of defects. At higher electrolyte temperatures, the oxide films on 304 stainless steel behave predominantly as an n-type conductor [3]. When higher anodic voltages are applied, the space charge region can be inverted to a p-type for an n-type conductor, and to an n-type for a p-type semiconductor [4]. The number of pits was greater when the films were of the n- type rather than the p-type [5]. Several researchers have intended to correlate the intrinsic properties of oxide films with pitting susceptibility, studying the semi conductive properties of oxides using AC impedance and photo electrochemical techniques. The photo-effect easily can be related to the semi conducting nature of the passive film. The concentration of carriers near the surface can be increased by illumination. Lenhard et al. [6] found a significant decrease in the number of pits and an increase in the breakdown potential, when the nickel oxide (p-type) was illuminated. At the same time the pitting potential moved to a more positive potential. The same phenomenon was found on steel [7]. Morach et al. [8] found that materials with a lower number of localized states have better resistance to localized corrosion. Bulk Al_2O_3 is an insulator with a band gap 8-9 eV [9] but the passive film on the Al exhibits a band gap ~ 3 eV [10]. Menezes et al. [10] measured the photocurrent as a function of potential for pure Al, and AA 7075 and AA 3003 alloys in chloride,

molybdate and sulfate solutions. They found that the flat band potential is dependent upon the kind of electrolyte present and shifts to a more positive value with increasing susceptibility to pitting, which is probably associated with a defect structure of the oxide (i.e., deviation from stoichiometry). According to the authors, the diminished photoresponse at positive potentials suggests that the defects (O vacancies or Al interstitials) migrate toward the interface and oxidize. Kobotiatis et al. [11] studied the electronic properties of a passive layer grown anodically on Al 70775 in chromate and oxalate solutions using electrochemical impedance spectroscopy. The Mott-Schottky plots were obtained from the measurements of capacitance at different potentials. Flat band potentials and the density of the energy state were calculated from these plots. Differences were found in semi conducting properties of the passive layer formed in chromate and oxalate solutions. These differences were related to the inhibition properties of chromate and oxalate to pitting. The oxide developed in the presence of chromate (good inhibitor) exhibits a less-noble flat-band potential and a lower average density of state. No effect of the electric potential was found on the flat band potential and the density of the energy states. Hence, in both of the above papers, the flat band potential was less noble in conditions when the susceptibility of Al to pitting is low as stated in the literature. The effect of the electronic structure on pitting can be explained by a point defect model [12]. This model assumes that the chloride ions incorporate to the passive film by occupying anion vacancies. This results in a decrease of anion vacancies and increases the cation vacancies. When the cation vacancies start to pile up at the metal interface, a breakdown of the films occurs. Initiation of localized corrosion upon high strength aluminum alloys is often associated with cathodic intermetallic particles within the alloy. Electrochemical measurements and metallurgical characterization have been made to clarify and quantify the physical properties of $\text{Al}_7\text{Cu}_2\text{Fe}$ particles in AA7075-T651. Prior studies regarding either the stereology or electrochemical properties of $\text{Al}_7\text{Cu}_2\text{Fe}$ are scarce. Quantitative microscopy revealed a significant population of $\text{Al}_7\text{Cu}_2\text{Fe}$ in the alloy; comprising up to 65% of the constituent particle population and typically at a size of $1.7 \pm 1.0 \mu\text{m}$. It was determined that $\text{Al}_7\text{Cu}_2\text{Fe}$ may serve as a local cathode in the evolution of localized corrosion of AA7075-T651 and is capable of sustaining oxygen reduction reactions at rates of several hundreds of $\mu\text{A}/\text{cm}^2$ over a range

of potentials typical of the open circuit potential (OCP) of AA7075-T651 in NaCl solution of various concentrations and pH. The presence of Al₇Cu₂Fe leads to the development of pitting at the particle–matrix interface.

2.2 Effect of cryo-rolling on corrosion behavior

From a viewpoint of metallurgy, corrosion is particularly associated with structural inhomogeneity due to precipitates, interfaces and other lattice defects. One of the most dangerous localized damage is intergranular corrosion associated with grain boundaries. Since the volume fraction of grain boundaries and lattice defects (residual dislocations) in the cryo-rolled material is very large, the acceleration of corrosion is expected. Besides, a large portion of the elastic energy is stored in heavily deformed materials as in the cryo-rolled Al. Therefore, it is reasonable to expect a higher dissolution rate in the UFG Al when compared to annealed or coarse-grain samples. High internal stresses and residual dislocations within the grains may also facilitate general matrix corrosion in the UFG state. A large volume fraction of non-equilibrium grain boundaries and high stresses inside the grains could result in homogeneous corrosion. Under these conditions it is quite plausible that a suitable annealing (recovery and recrystallization) could improve the corrosion properties of these samples (UFG samples), as evinced by the corrosion data. The partially recrystallized state of the samples could have enhanced the corrosion in the samples annealed at 195°C. The microscopic surface observation after the polarization tests did not clearly reveal the corrosion localization. However, it is believed that the corrosion localization along the boundaries could be high in cryo processed samples due to high residual dislocation density and a large volume fraction of interfaces in the matrix. It is emphasized here that further detailed investigations are required in both electrochemical and metallurgical aspects of cryo-rolling processed metals.

2.3 Metallurgical tempers of high-strength alloys

T3	Solution heat-treated, cold-worked, naturally aged
T4	Solution heat-treated, naturally aged
T6	Solution heat-treated, artificially aged
T76	Solution heat-treated, artificially aged to provide good resistance to exfoliation corrosion
T736	Compromise between T73 and T76
T8	Solution heat-treated, cold worked, artificially aged
T..510	No further straightening after stretching (extrusion)
T..511	Minor straightening after stretching to comply with standard tolerances (extrusion)
T..52	Stress-relieved by compressing

2.4 Corrosion behavior

- Avoid using alkaline cleaning media.
- Possible addition to use corrosion inhibitors (Natrium silicates $n\text{SiO}_2, \text{Na}_2\text{O}$) in OH^- containing solutions.
- Use of surface coating to prevent corrosion.

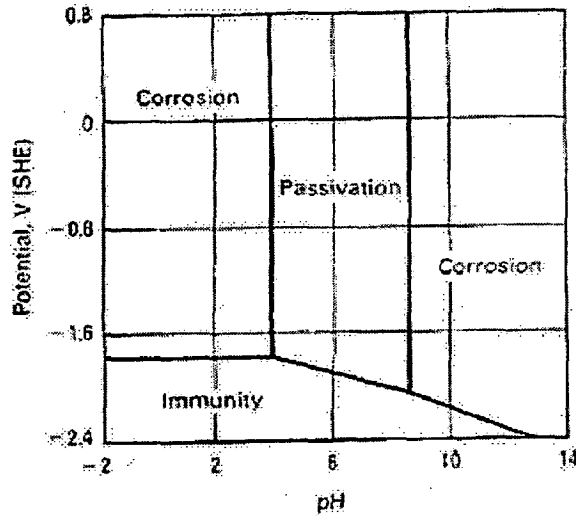


Fig 2.1 Pourbaix diagram for aluminium with $Al_2O_3 \cdot 3H_2O$ film at 25C. Potential values are for the standard hydrogen electrode (SHE) scale.

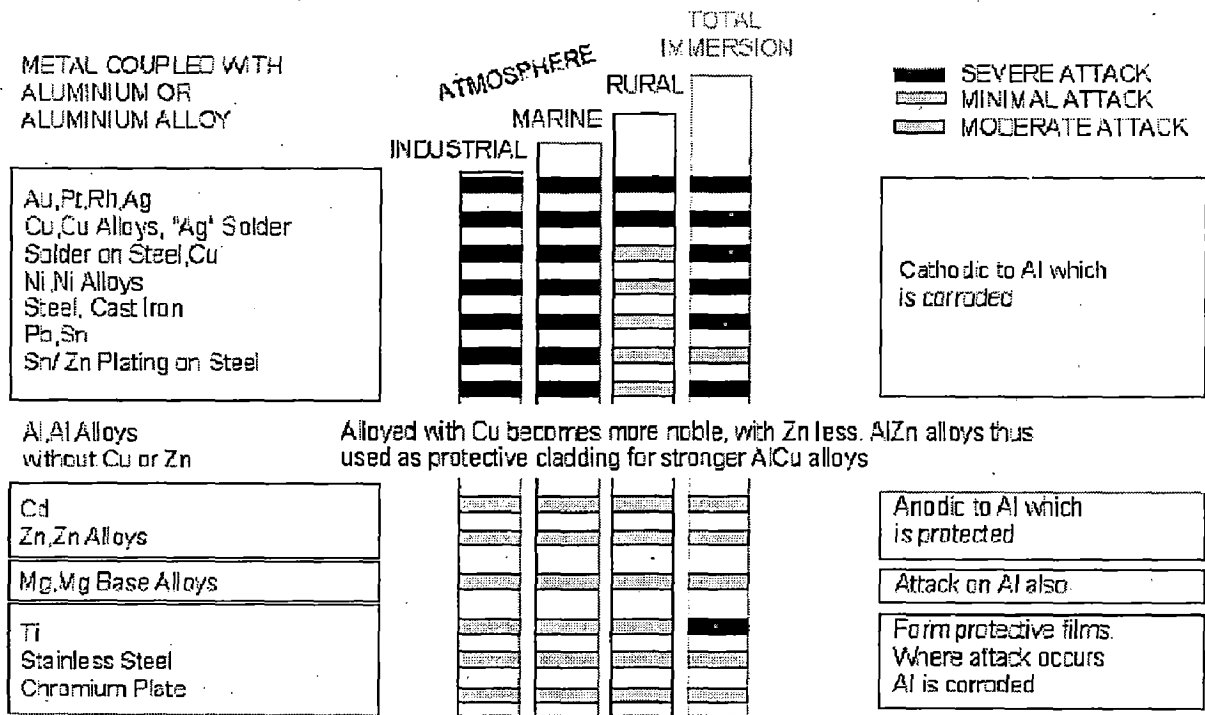


Fig. 2.2 Corrosion behavior under different environment.

2.5 Stress cracking corrosion

Only aluminium alloys that contain appreciable amounts of soluble alloying elements, primarily copper, magnesium, silicon, and zinc, are susceptible to SCC. These include the heat treatable 2XXX and 7XXX alloys and 5XXX alloys containing >3%Mg. For most commercial alloys, tempers have been developed that provide a high degree of immunity to SCC in many environments. Stress corrosion cracking behavior is strongly dependent on both the heat treatments and composition of alloy. Tabulations of relative susceptibilities of aluminium alloys are available in ASTM G 64, "classification of resistance to stress-corrosion cracking of high strength aluminium alloys. Other important considerations include the effects of grain structure and stress direction. Many wrought aluminium alloy products have highly directional grain structures. Such products are highly anisotropic with respect to resistance to SCC. Resistance, which is measured by magnitude of tensile stress required to cause cracking, is highest when the stress is applied in the longitudinal direction, lowest in traverse direction, and intermediate in other directions. These differences are most noticeable in the more susceptible tempers but are usually much lower in tempers produced by extended precipitation treatments, such as T6 and T8 tempers for 2XXX alloys and T73, T736, and T76 tempers for 7XXX alloys.

2.6 Corrosion inhibition of aluminium alloys by rare earth chlorides

Aluminum and its alloys are widely used in engineering applications because of their low density, favorable mechanical properties, good surface finish and relatively good corrosion resistance. Research efforts in the aeronautical industry have focused on the study of Al-Cu and Al-Zn alloys. The electrochemical behavior of Al and its alloys has attracted the attention of many investigators. The natural oxide film on aluminum does not offer sufficient protection against aggressive anions. In this context, inhibitors are used to improve protective features of the surface. Currently, chromates are widely used in anticorrosive pre-treatments of aluminum alloys [24]. However, because of their high toxicity, an intense research effort is underway for their replacement. Rare earth chlorides have been tested as corrosion inhibitors for Al alloys like AA5083 [25], AA7075 [26], AA8090 [27], AA6061 [28] and AA2024 [29]. These rare earth chlorides

act as cathodic inhibitors [30]. Bethencourt et al. [31] observed, from weight loss and polarization results, that lanthanum, cerium and samarium chlorides are effective uniform corrosion inhibitors of AA5083 in aerated 3.5% NaCl solution. As no pits were observed in samples immersed in solutions containing inhibitors, they concluded that these rare earth salts also act as pitting corrosion inhibitors. Arnott et al. [32] investigated the corrosion inhibition behavior of 1000 ppm concentration of different rare earth chlorides (YCl_3 , PrCl_3 , LaCl_3 and CeCl_3) and other salts such as FeCl_2 , CoCl_2 and NiCl_2 , on AA7075 in 3.5% NaCl solution. The best degree of inhibition was achieved by CeCl_3 addition. Davo' and Damborenea [33] studied the effect of different concentrations of LaCl_3 and CeCl_3 on the corrosion of AA 8090 in 3.56% NaCl solution. Maximum inhibition was obtained after addition of 1000 ppm CeCl_3 and 250 ppm LaCl_3 . Cerium chloride inhibited intergranular corrosion more effectively than lanthanum chloride. Neil and Garrard [34] studied the effect of cerium pre-treatments on AA6061 prior to immersion in 3.5% NaCl solution. They immersed the samples in 0.1 M NaCl/1000 ppm CeCl_3 solution for one week and then transferred them to the test solution. They concluded that cerium pre-treatment decreased the corrosion susceptibility, but the effect of the treatment was short lived. Aldykewicz et al. [35] reported that the corrosion inhibition of cerium chloride addition in NaCl solution was related to the development of a cerium-rich film over the cathodic copper surface in the case of AA2024. Aballe et al. [36] analyzed the effect of CeCl_3 , LaCl_3 and mixture of both CeCl_3 and LaCl_3 on the corrosion of AA 5083 alloy in NaCl solution. They found that corrosion resistance offered by these rare earth metal chlorides was of same order as those found with classical Cr-based compounds. They further observed that there was a two-fold increase in polarization resistance after addition of 500 ppm LaCl_3 , four-fold after 500 ppm CeCl_3 and nearly six-fold after addition of 250 ppm each of LaCl_3 and CeCl_3 . They concluded that mixed solutions of LaCl_3 and CeCl_3 in optimum ratio showed a better performance than solely $\text{LaCl}_3/\text{CeCl}_3$ inhibitor.

Recently, ultra/nano fine grained (UFG) materials with the grain size less than 1 μm have been studied extensively, since they provide high strength without the degradation of toughness. The previous works showed that severe plastic deformation (SPD) techniques, such as equal channel angular pressing, accumulative roll bonding, multiple compression, and severe torsional straining, etc., are effective on manufacturing UFG materials [1–5]. However, the existing SPD processes require a large amount of plastic deformation and special procedures. Meanwhile, deformation at the cryogenic temperature also has the potential producing bulk UFG materials. The suppression of dynamic recovery during deformation at extremely low temperatures is expected to preserve a high density of defects generated by deformation, which can act as the potent recrystallization sites. Accordingly, the cryogenic deformation would require less plastic deformation for achieving ultra fine grains, compared to the SPD processes at ambient or elevated temperatures. For instance, Wang et al. [6] obtained UFG pure copper by applying cryogenic rolling (cryo-rolling). Further, they reported that the bimodal microstructure of ultra fine grains and relatively coarse grains obtained by cryo-rolling followed by low temperature annealing resulted in the excellent combination of ultrahigh strength and ductility. Similarly, the application of cryo-rolling to the commercial Al alloys is anticipated to refine their grains to the sub-micrometer level, i.e. UFG structure, with less plastic deformation than the SPD processes. Although mechanical behavior of ultrafine grained Al alloys produced by cryo-rolling is reported in the literature, their corrosion behavior is scanty in the literature. Owing to the aforementioned facts, the present work has been focussed to study the corrosion behavior of an Al-Mg-Si alloys (6063 Al alloys) rolled at the cryogenic temperature. Due to low weight of aluminium alloys, it is extensively used in aerospace and automobile applications and by cryo-rolling; we can further reduce their weight and increase the strength. But at the same time, ultra fine grains that is number of grains per unit area increases, which directly affect the corrosion resistance. With an increase in volume fraction of grain boundary area, corrosion tendency of material are expected to change significantly. Hence, the

4.1 Materials formulation

The materials for the present study, namely ultrafine/nano grained aluminium alloys processed by cryo-rolling with thickness reduction of 35%, 47%, 55%, 80%, 90% respectively were provided by Hindalco industries limited ,Aditya Birla group, Renukoot (India) in the rolled sheet form. The specimens with dimensions of approximately 20mm x 15mmx 0.2mm, 20 mm x15 mm x 1.2 mm, 20 mm x15 mm x3.6 mm, 20 mm x15 mm x4 mm, 20 mm x 15 mm x 5.9 mm respectively, each having five pieces were cut from the alloy sheets.

- **Materials specifications**

Nominal composition by Wt. % of Cr-Al-alloys is reported in table 4.1

Table 4.1 Nominal composition by Wt. % of Cr-Al-alloys.

Alloy/elements	Si	Mg	Cu	Mn	Fe	Zn	Cr
CR-Al-alloys	0.45	0.3	0.05	0.013	0.048	0.022	0.022

- **Product characteristics**

- * It has high strength and ductility.

- *Electrical conductivity of the cryo-rolled samples decreased due to increased number of electron scattering centers (lattice defects and grain boundary area).

- **Applications:** structural aircraft applications.

4.2 Sample preparation

Samples were cut into the size of 20mmx15mmx0.2mm, 20mmx15mmx1.2mm, 20mmx 15mmx 3.6mm, 20mmx15mmx4mm, 20mmx15mmx5.9mm out of the rolled sheet provided. Samples were wheel grinded, then on the Sic papers down to 1000grits and polished on 1/0,2/0,3/0,4/0 grade and then cloth polished for 2 minutes and that cleaned with acetone.

4.3 Salt spray machine:

The salt solution is prepared by dissolving 3.5% \pm 1 parts by mass of sodium chloride in 95 parts of water conforming to Type IV water in Specification D 1193 (except that for this practice limits for chlorides and sodium may be ignored). Careful attention is given to the chemical content of the salt. The salt used was sodium chloride with not more than 0.3 % by mass of total impurities. Halides (Bromide, Fluoride, and Iodide) other than Chloride constitute less than 0.1 % by mass of the salt content. Copper content is less than 0.3 ppm by mass. Sodium chloride containing anti-caking agents is not used because such agents may act as corrosion inhibitors. See Table 4.2 for a listing of these impurity restrictions.

Table 4.2 Maximum Allowable Limits for Impurity Levels in NaCl.

Impurity Description	Allowable Amount
Total Impurities	\leq 0.3 %
Halides (Bromide, Fluoride and Iodide) excluding Chloride	\leq 0.1 %
Copper	\leq 0.3 ppm
Anti-caking Agents	0.0 %

The pH of the salt solution when atomized at 35°C (95°F), vary from 6.5 to 7.2. Before the solution is atomized, it should be free of suspended solids. The pH measurement is made at 25°C (77°F) using a suitable glass pH-sensing electrode, reference electrode, and pH meter system in accordance with Test Method E 70. The exposure zone of the salt spray chamber is maintained at 35 \pm 1.1 - 1.7°C (95 \pm 2 - 3°F).

4.4 Salt spray corrosion tests

The specimens are exposed to cyclic corrosion tests for 24 hours, 48 hours, and 72 hours respectively. The temperature for salt chamber is around 35° C and that of tank temperature is around 45° C. After each duration of the test, the weight of test specimen was measured using an electronic weighing balance. The weight change to determine the total rate of corrosion. The efforts were made to formulate the kinetics of corrosion. The samples after corrosion were analyzed using SEM, XRD and FESEM for surface and phase analysis.

4.5 Sources of error

1. Inaccurate calibration of temperature inside salt chamber.
2. Interruptions in exposure, cause, and length of time.
3. Electricity power cut during the operation.

4.6 Precautions

1. Unless otherwise specified, the specimens shall be supported or suspended between 15 and 30° from the vertical preferably parallel to the principal direction of flow of fog through the chamber, based upon the dominant surface being tested.

2. The specimens shall not contact each other or any metallic material or any material capable of acting as a wick.

3. Each specimen shall be placed to permit unencumbered exposure to the fog.

4. Salt solution from one specimen shall not drip on any other specimen.

5. When the pH of a salt solution is adjusted at room temperature, and atomized at 35°C (95°F), the pH of the collected solution will be higher than the original solution due to the loss of carbon dioxide at the higher temperature. When the pH of the salt solution is adjusted at room temperature, it is therefore necessary to adjust it below 6.5 so the collected solution after atomizing at 35°C (95°F) will meet the pH limits of 6.5 to 7.2. Take about a 35-mL sample of the salt solution as prepared at room temperature, boil gently for 30 s, cool, and determine the pH. When the pH of the salt solution is adjusted to 6.5 to 7.2 by this procedure, the pH of the atomized and collected solution at 35°C (95°F) will come within this range.

6. Heating the water from which the salt solution is prepared to 35°C (95°F) or above, to expel carbon dioxide, and adjusting the pH of the salt solution within the limits of 6.5 to 7.2 produces a solution the pH of which does not materially change when atomized at 35°C (95°F).

7. The freshly prepared salt solution may be filtered or decanted before it is placed in the reservoir, or the end of the tube leading from the solution to the atomizer may be covered with a double layer of cheese cloth to prevent plugging of the nozzle.

8. The air supply may be freed from oil and dirt by passing it through a suitable oil/water extractor (that is commercially available) to stop any oil from reaching the Air

Saturator Tower. Many oil/water extractors have an expiration indicator, proper preventive maintenance intervals should take these into account.

9. A suitable method to record the temperature is by a continuous recording device or by a thermometer which can be read from outside the closed cabinet. The recorded temperature must be obtained with the salt spray chamber closed to avoid a false low reading because of wet-bulb effect when the chamber is open.

4.7 Salt immersion tests

The cryo-rolled Al alloys were subjected to immersion tests for 14 days in water-salt solutions contained 3.5% NaCl. After 14 days test, the weight of test specimen was measured using a electronic weighing balance. The spalled scale was not included at the time of measurement of the weight change to determine the total rate of corrosion. The efforts were made to formulate the kinetics of corrosion.

5.1. Visual observation

Immersion results

The three different thickness of ultrafine grained aluminium alloys processed by cryo-rolling in 3.5% NaCl solution has shown spalling right from the first day onwards which slightly increased as the period of study progressed with lot of corrosion products found in the beaker. The surface became rougher with the progress of study at some places which shows that localized type of corrosion have been taken place. The color of the oxide formed on the surface was whitish in color which loosely adherent to the surface and after sometime it was spalled into the solution. We have seen that smaller thickness specimen undergo larger corrosion rate as compared to larger thickness specimen.

Salt spray test results for 24 hours

The five different thickness ultrafine grained Al-Mg-Si alloys processed by cryo-rolling has been kept in salt spray chamber spraying 3.5% salt solution continuously for 24 hours. The corrosion products are found on surface of the samples. The surface became rougher at some places which may be due to that the localized type of corrosion attack. The scale formed on the surface was whitish in color and it was loosely adherent to the surface. It has been seen that corrosion rate increases with the decrease in the thickness of specimen.

Salt spray test results for 48 hours

The five different thickness ultrafine grained aluminium alloys processed by cryo-rolling has been put in a salt spray chamber and 3.5% salt solution was continuously sprayed over the samples for 48 hours. The corrosion products are found on the surface of the samples. The surface become rougher at some places which shows that localized type of corrosion has taken place. The scale which has formed on the surface was whitish in color and it was loosely adherent to the surface. It was observed that corrosion rate

increases with the decrease in the thickness of specimen. But as compared to 24 hours test the extent of corrosion was comparatively less.

Salt spray test results for 72 hours

The five different thickness ultrafine grained aluminium alloys processed by cryo-rolling has been kept in salt spray chamber spraying 3.5% salt solution continuously for 72 hours. The corrosion products are found on the surface of the samples. The surface became rougher at some places showing the localized type of corrosion attack. The scale formed on the surface was whitish in color and it was loosely adherent to the surface. It was observed that the corrosion rate increases with the decrease in the thickness of specimen. But as compared to 48 hours test, the extent of corrosion was comparatively less.

5.2. Thermo gravimetric analysis

Using immersion test, it is shown that weight change (mg/dm^2) for smaller thickness material is greater than larger thickness material. The data obtained after 14 days of test are tabulated in Table 5.1.

Table 5.1 Thermo gravimetric data for immersion test

Original weight(mg)	Cumulative Weight loss(mg)	Corrosion rate in mdd i.e. in $\text{mg}/(\text{day}\cdot\text{dm}^2)$
127	4	4.76×10^{-6}
844	3.5	6.9×10^{-5}
3189	1.8	1.19×10^{-5}

The above data shows that in 3.5% salt solution, the cumulative weight loss (mg) in smaller thickness specimen was larger as compared to larger thickness specimen.

Using the salt spray test for 24 hours, 48 hours, 72 hours duration respectively, it is evident that weight change (mg/dm^2) for the same thickness specimen increases with

the increase of duration of test. But, for the same duration test for different specimen thickness decreases with increase in thickness. The data obtained are given in Table 5.2.

Table 5.2 Thermo gravimetric data for salt spray test for 24 hours

Original Wt.(mg)	Cumulative Wt. loss (mg)	Corrosion rate in mdd
127	4	6.6×10^7
844	3.5	9.7×10^6
3189	1.8	1.6×10^6
3262.3	1.2	1×10^6
4546.2	1	5.64×10^5

Table 5.3 Thermo gravimetric data for salt spray test for 48 hours

Original Wt.(mg)	Cumulative Wt. loss (mg)	Corrosion rate in mdd
127	8	6.6×10^7
844	6	8.3×10^6
3189	3	1.38×10^6
3262.3	2.3	9.58×10^5
4546.2	1.9	5.37×10^5

Table 5.4 Thermo gravimetric data for salt spray test for 72 hours

Original Wt.(mg)	Cumulative Wt. loss (mg)	Corrosion rate in mdd
127	10	5.5×10^7
844	8	7.4×10^6
3189	3.9	1.2×10^6
3262.3	3.3	9.16×10^5
4546.2	2.7	5.08×10^5

Steady state condition is achieved after a long period of exposure. From the above discussion, it is evident that the specimen of smaller thickness undergoes higher cumulative weight loss while the larger thickness materials undergo less cumulative weight loss. The smaller specimen undergo higher corrosion rate while large thickness material undergo lesser corrosion rate. The reason for this that with cryo-rolling number of grains per unit area increases with thickness reduction and corrosion resistance inversely related to number of grains per unit area.

5.3 X-ray Diffraction Analysis

Different samples as obtained after exposure to various environments were subjected to XRD analysis to identify various phases formed on their surfaces. Diffraction patterns were obtained by Burker AXS D-8 Advance Diffractometer (Germany) with CuK_α radiation and Ni filter at 20 ma under a voltage of 20 to 120 and intensities were recorded at a chart speed of 2cm/min with 2/min as Goniometer speed. For the intensity peaks and corresponding values of 2θ , the interplaner spacing-d, has been calculated using bragg's law.

$$2d\sin\theta=n\lambda$$

The different-d values obtained were used to identify various phases with the help of inorganic ASTM X-Ray diffraction data card.

24 hours salt spray tests

Sample of thickness t_1 :- The obtained “d” values showed the presence of CuAl_2O_4 , $\alpha\text{-Al}_2\text{O}_3\cdot\text{H}_2\text{O}$ and $\text{FeO}\cdot\text{Cr}_2\text{O}_3$ as major phases. **Fig 5.1**

Sample of thickness t_2 :- The obtained “d” values showed the presence of $\text{Mg}_{5.37}\text{Al}_{8.61}\text{Fe}_{1.92}(\text{Al}_{5.66}\text{Be}_{1.47}\text{Fe}_{0.07}\text{Si}_{4.80})\text{O}_{40}$, $\text{CrO}_{0.87}$, $\text{Al}_2\text{O}_3\cdot\text{H}_2\text{O}$ and CuAl_2O_4 as major phases. **Fig 5.2**

Sample of thickness t_3 :- The obtained “d” values showed the presence of $\text{CrO}_{0.87}$ and aluminum oxide as major phases. **Fig 5.3**

Sample of thickness t_4 :- The obtained “d” values showed the presence of $(\text{Mg}_{5.67}\text{Al}_{8.61}\text{Fe}_{1.92})(\text{Al}_{5.66}\text{Be}_{1.47}\text{Fe}_{0.07}\text{Si}_{4.8})\text{O}_{40}$, aluminum oxide and silicon oxide as major phases. **Fig 5.4**

Sample of thickness t_5 :- The obtained “d” values showed the presence of $\text{Na}_5(\text{Al}(\text{OH})_6)(\text{OH})_2$, aluminum oxide and silicon oxide as major phases. **Fig 5.5**

48 hours salt spray tests

Sample of thickness t_1 :- The obtained “d” values showed the presence of $\text{FeO}\cdot\text{Cr}_2\text{O}_3$, aluminum oxide and iron oxide as major phases. **Fig 5.6**

Sample of thickness t_2 :- The obtained “d” values showed the presence of $\text{Cr}_2\text{O}_3\cdot\text{FeO}$, $\text{Mg}(\text{ClO}_4)_2\cdot 6\text{H}_2\text{O}$, $\text{Na}_2\text{SiO}_3\cdot 9\text{H}_2\text{O}$, $\text{FeO}\cdot\text{Cr}_2\text{O}_3$, CuAl_2O_4 , $\text{Mg}(\text{Al}_{0.91}\text{Fe}_{0.09})\text{O}_4$ and $\text{Cr}_2\text{O}_3\cdot\text{FeO}$ as major phases. **Fig 5.7**

Sample of thickness t_3 :- The obtained “d” values showed the presence of $\text{Al}_2\text{O}_3\cdot 3\text{H}_2\text{O}$, CuAl_2O_4 , $\text{Mg}(\text{Al}_{0.91}\text{Fe}_{0.09})\text{O}_4$, $\text{Mg}(\text{ClO}_4)_2\cdot 6\text{H}_2\text{O}$, $\text{FeO}\cdot\text{Cr}_2\text{O}_3$ and $\text{Cr}_2\text{O}_3\cdot\text{FeO}$ as major phases. **Fig 5.8**

Sample of thickness t_4 :-The obtained “d” values showed the presence of $\text{Al}_2\text{O}_3\cdot\text{H}_2\text{O}$, $\text{Zn}(\text{AlO}_2)_2$, CuAl_2O_4 , $\text{Al}_2\text{O}_3\cdot 0.33\text{H}_2\text{O}$, and $\text{Mg}(\text{Al}_{0.91}\text{Fe}_{0.91})\text{O}_4$ as major phases. **Fig 5.9**

Sample of thickness t_5 :- The obtained “d” values showed the presence of $\text{Al}_2\text{O}_3\cdot\text{H}_2\text{O}$, $\text{Zn}(\text{AlO}_2)_2$, CuAl_2O_4 , $\text{Mg}(\text{Al}_{0.91}\text{Fe}_{0.09})\text{O}_4$, $\text{FeO}\cdot\text{Cr}_2\text{O}_3$ and $\text{Cr}_2\text{O}_3\cdot\text{FeO}$ as major phases. **Fig 5.10**

72 hours salt spray tests

Sample of thickness t_1 :- The obtained “d” values showed the presence of $\text{Al}_2\text{O}_3\cdot\text{H}_2\text{O}$, $\text{Zn}(\text{AlO}_2)_2$, $\text{Cu}(\text{Al}_2\text{O}_4)$, MgAl_2O_4 , Cl_2O , $\text{FeO}\cdot\text{H}_2\text{O}$ and $\text{Cr}_2\text{O}_3\cdot\text{FeO}$ as major phases. **Fig 5.11**

Sample of thickness t_2 :- The obtained “d” values showed the presence of $\text{Al}_2\text{O}_3\cdot\text{H}_2\text{O}$, $\text{Zn}(\text{AlO}_2)_2$, CuAl_2O_4 , MgAl_2O_4 , $\text{Mg}(\text{Al}_{0.91}\text{Fe}_{0.09})\text{O}_4$, $\text{FeO}\cdot\text{Cr}_2\text{O}_3$, and $\text{Mg}(\text{ClO}_4)2.6\text{H}_2\text{O}$ as major phases. **Fig 5.12**

Sample of thickness t_3 :- The obtained “d” values showed the presence of $\text{Al}_2\text{O}_3\cdot\text{H}_2\text{O}$, $\text{Zn}(\text{AlO}_2)_4$, $\text{Cu}(\text{Al}_2\text{O}_4)$, MgAl_2O_4 , $\text{Al}_2\text{O}_3\cdot 0.33\text{H}_2\text{O}$, $\text{FeO}\cdot\text{Cr}_2\text{O}_3$ and $\text{Mg}(\text{ClO}_4)2.6\text{H}_2\text{O}$ as major phases. **Fig 5.13**

Sample of thickness t_4 :- The obtained “d” values showed the presence of $\text{Al}_2\text{O}_3\cdot\text{H}_2\text{O}$, $\text{Zn}(\text{AlO}_2)_2$, $\text{Cu}(\text{Al}_2\text{O}_4)$, $\text{Mg}(\text{Al}_{0.91}\text{Fe}_{0.09})\text{O}_4$ and $\text{FeO}\cdot\text{Cr}_2\text{O}_3$ as major phases. **Fig 5.14**

Sample of thickness t_5 :- The obtained “d” values showed the presence of $\text{Al}_2\text{O}_3\cdot\text{H}_2\text{O}$, $\text{Zn}(\text{AlO}_2)_2$, CuAl_2O_4 , MgAl_2O_4 , $\text{Mg}(\text{Al}_{0.91}\text{Fe}_{0.09})\text{O}_4$, $\text{Al}_2\text{O}_3\cdot\text{H}_2\text{O}$ and $\text{Cr}_2\text{O}_3\cdot\text{FeO}$ as major phases. **Fig 5.15**

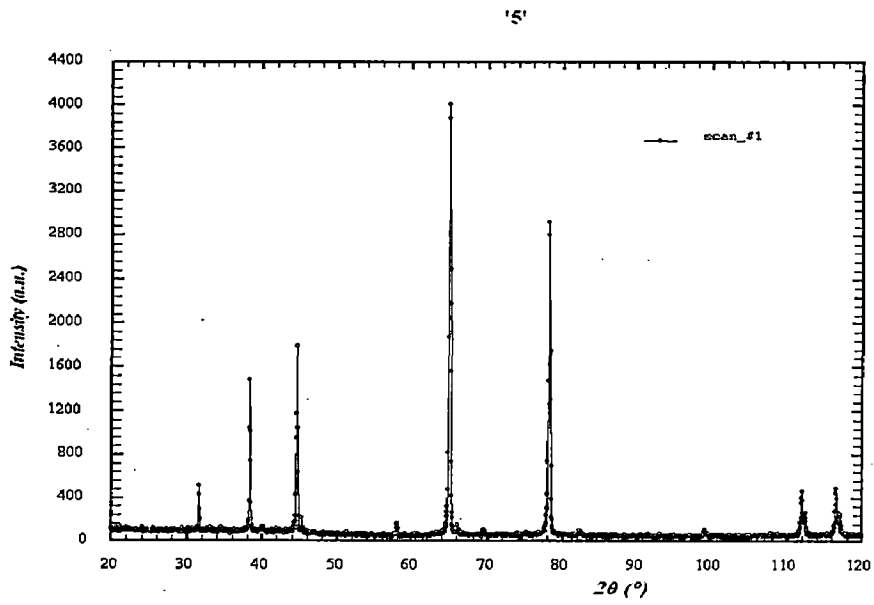


Fig 5.1 XRD pattern for 24 hours salt spray test for specimen thickness t_1

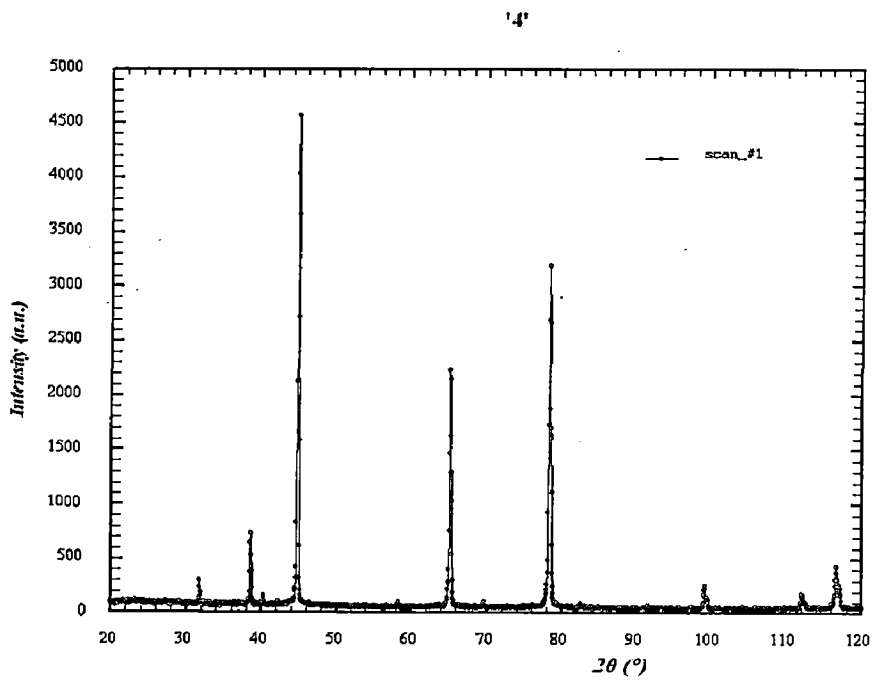


Fig 5.2 XRD pattern for 24 hours salt spray test for specimen thickness t_2

'3'

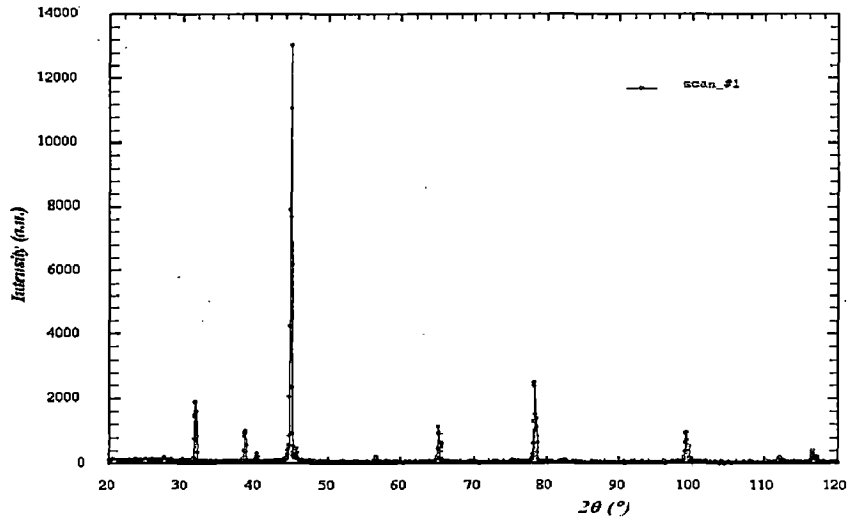


Fig 5.3 XRD pattern for 24 hours salt spray test for specimen thickness t_3

'2'

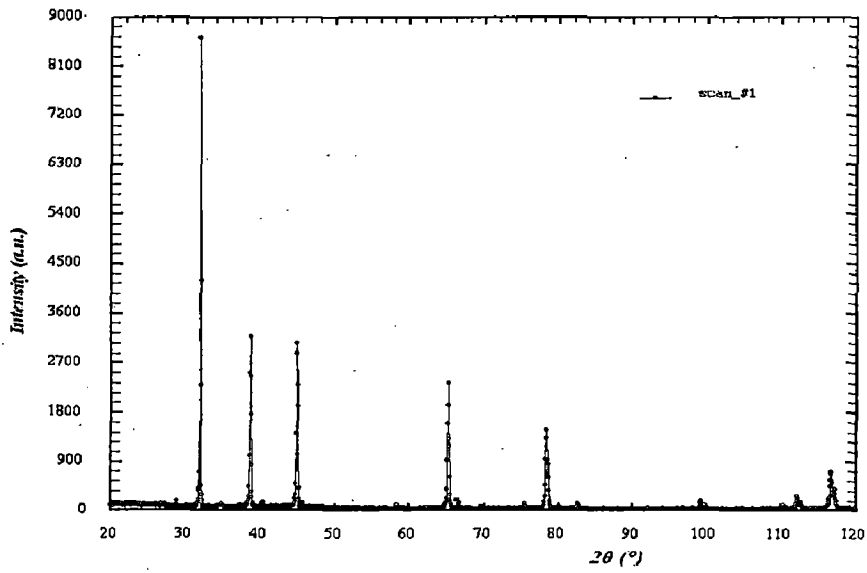


Fig 5.4 XRD pattern for 24 hours salt spray test for specimen thickness t_4

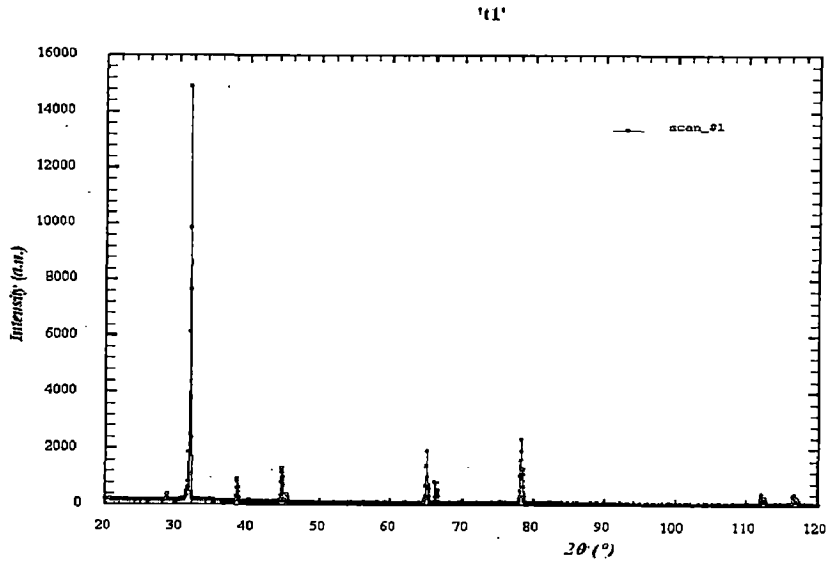


Fig 5.5 XRD pattern for 24 hours salt spray test for specimen thickness t_5

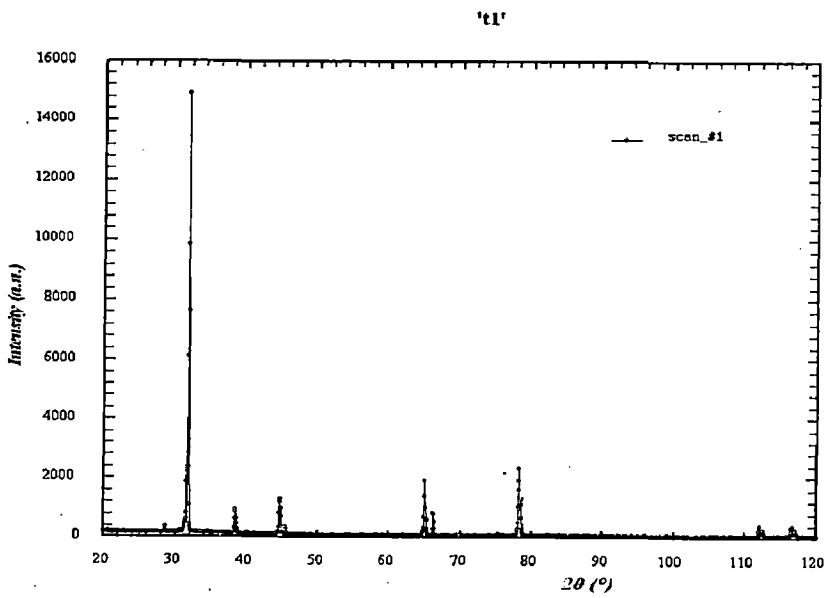


Fig 5.6 XRD pattern for 48 hours salt spray test for specimen thickness t_1

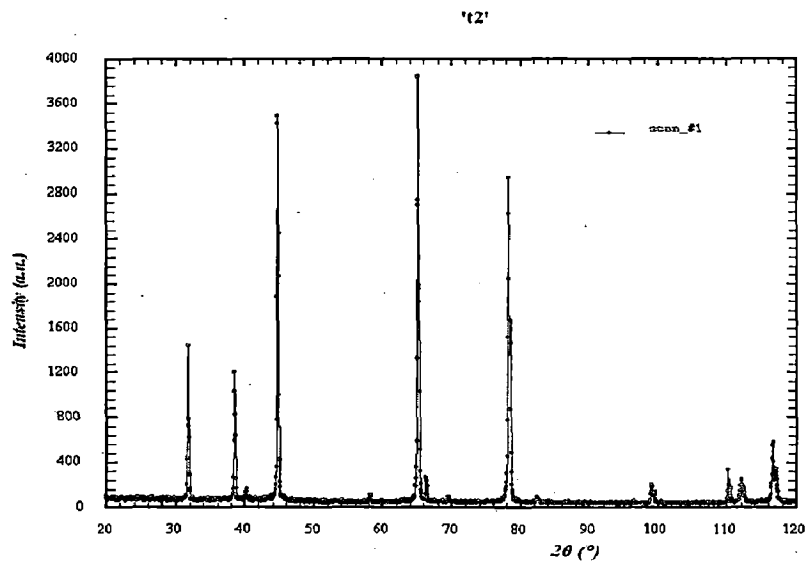


Fig 5.7 XRD pattern for 48 hours salt spray test for specimen thickness t_2

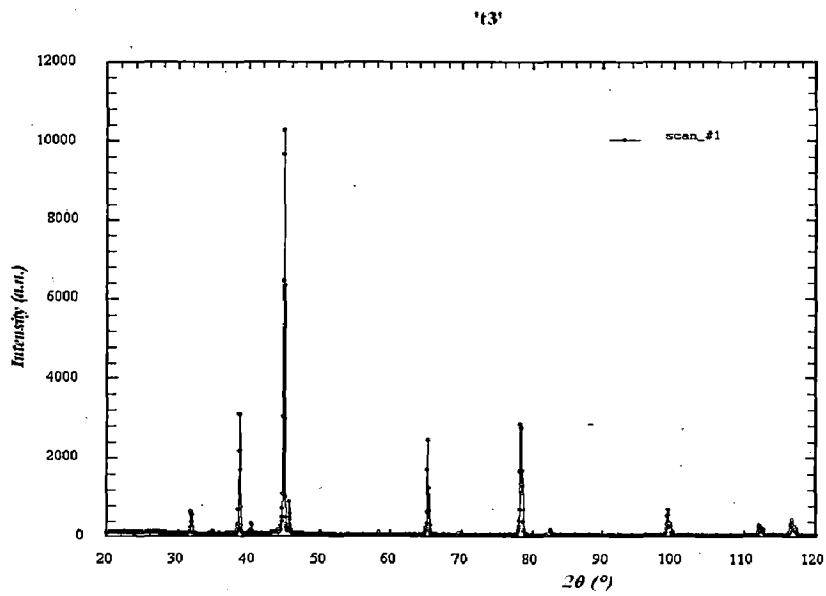


Fig 5.8 XRD pattern for 48 hours salt spray test for specimen thickness t_3

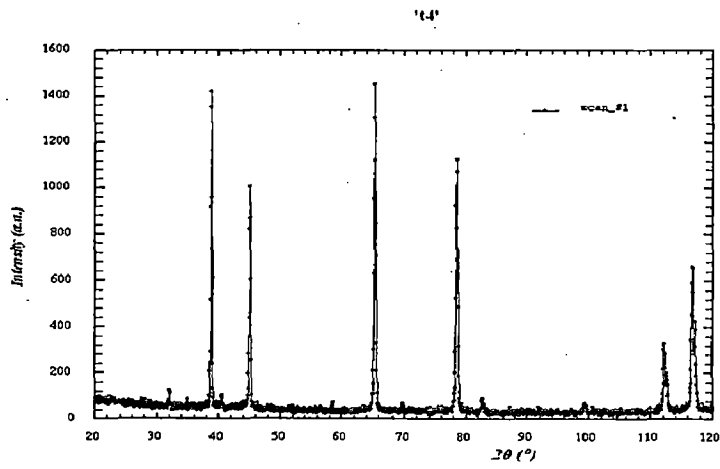


Fig 5.9 XRD pattern for 48 hours salt spray test for specimen thickness t_4

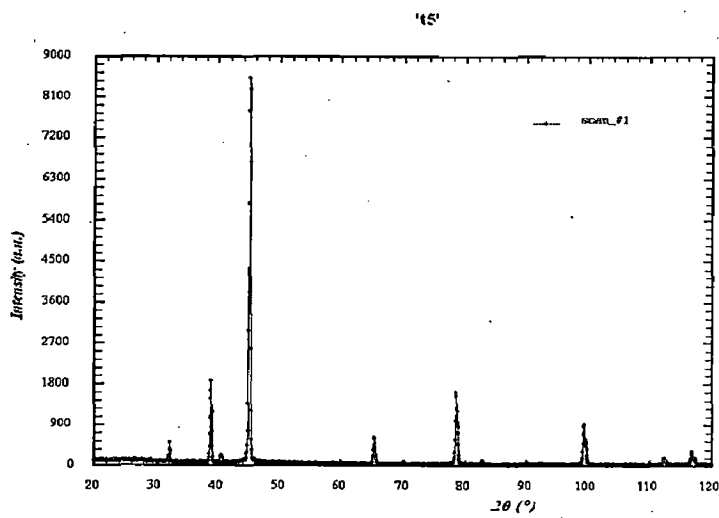


Fig 5.10 XRD pattern for 48 hours salt spray test for specimen thickness t_5

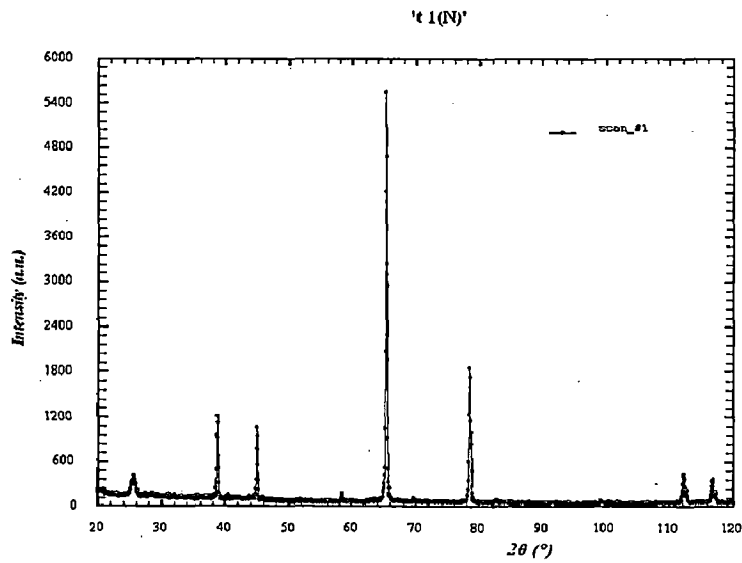


Fig 5.11 XRD pattern for 72 hours salt spray test for specimen thickness t_1

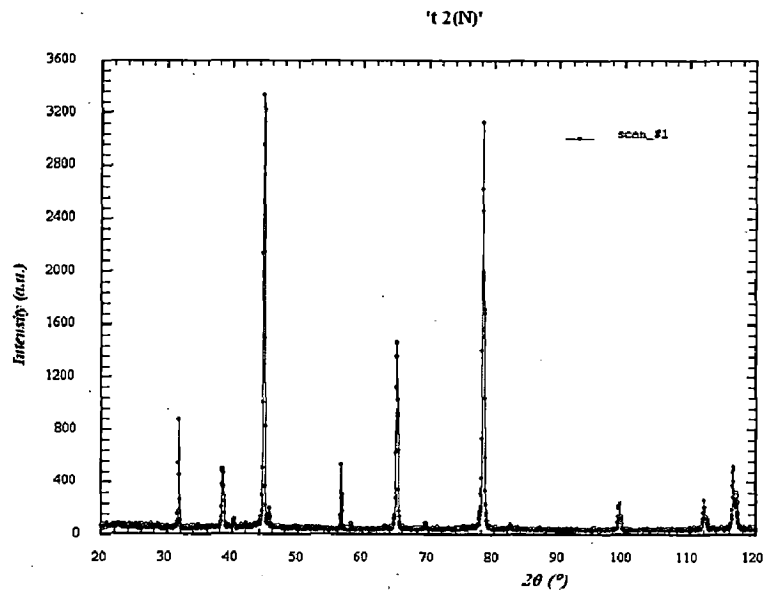


Fig 5.12 XRD pattern for 72 hours salt spray test for specimen thickness t_2

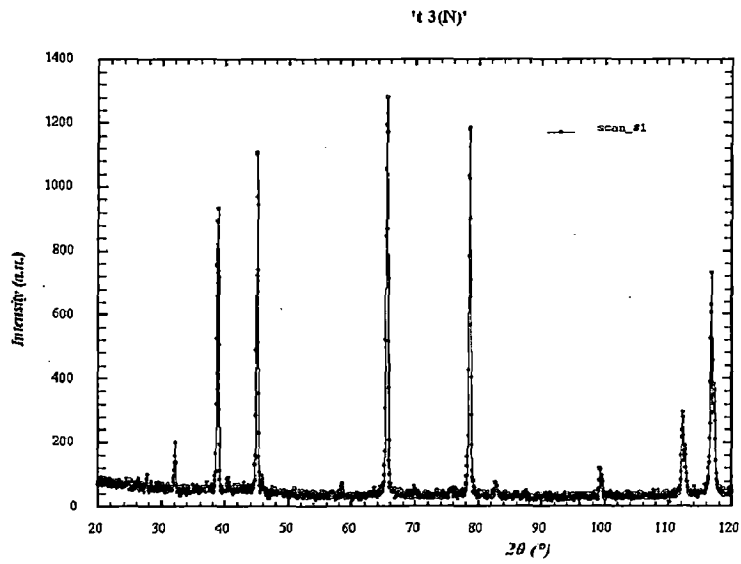


Fig 5.13 XRD pattern for 72 hours salt spray test for specimen thickness t_3

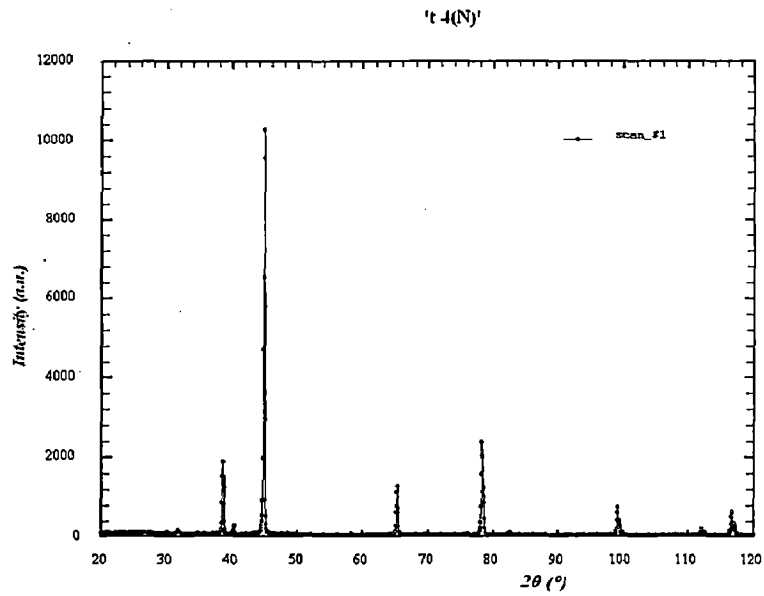


Fig 5.14 XRD pattern for 72 hours salt spray test for specimen thickness t_4

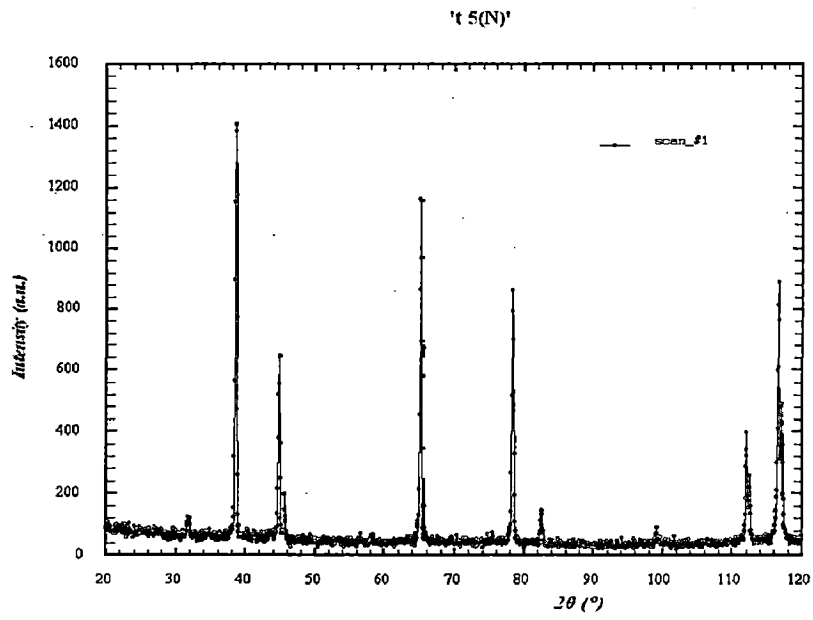
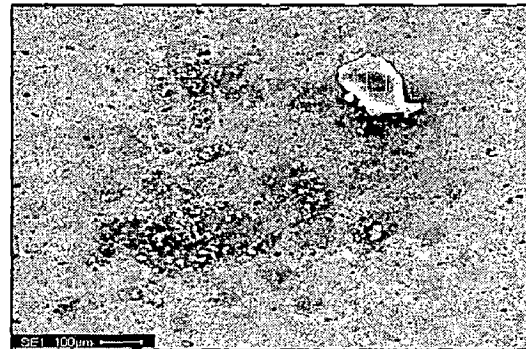
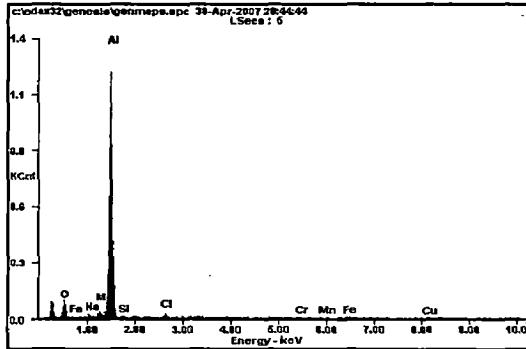


Fig 5.15 XRD pattern for 72 hours salt spray test for specimen thickness t_5

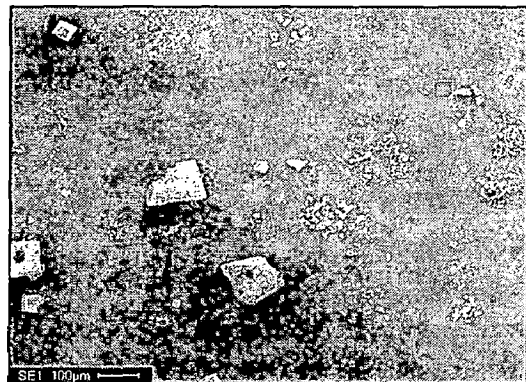
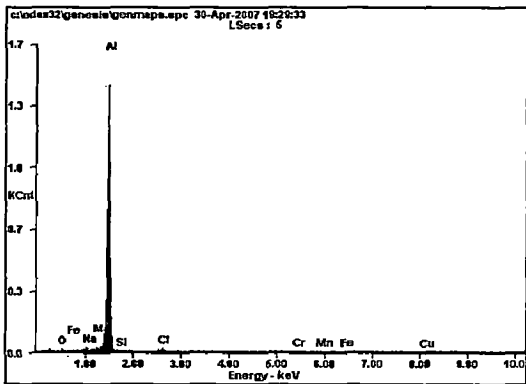
5.4 FESEM Results

The corroded specimens were mounted in resin to obtain FESEM images. FESEM images reveal the surface morphology and give the phases present in the scale.

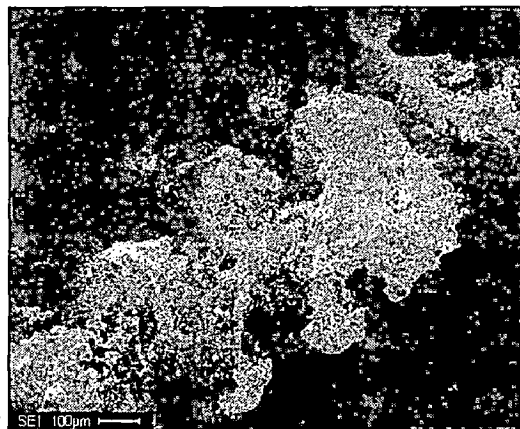
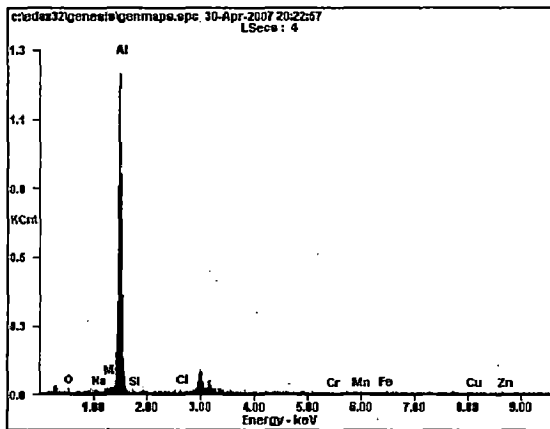
FESEM results for specimens undergo 24 hours duration test



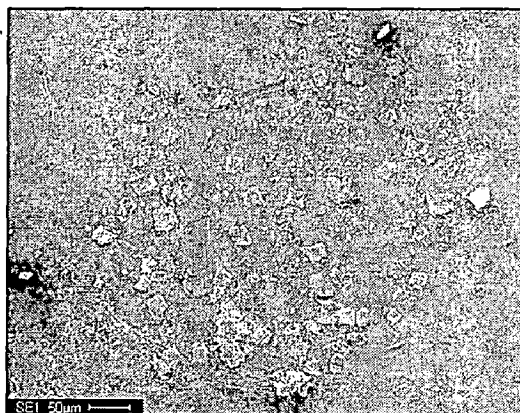
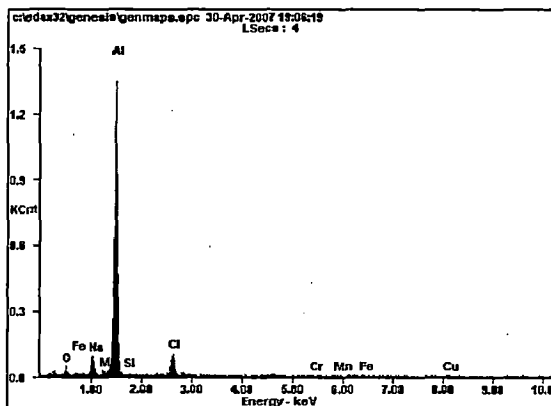
5.16 EDAX pattern and its SEM image of specimen of thickness t_1



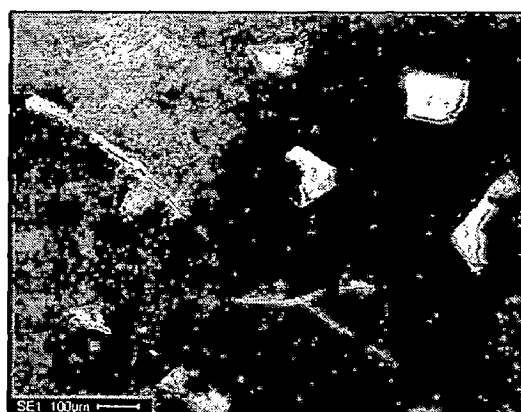
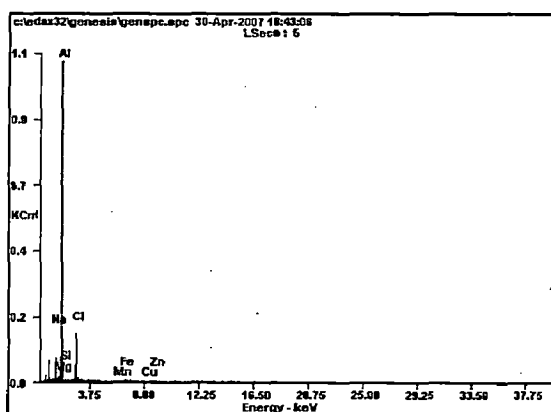
5.17 EDAX pattern and its SEM image of specimen of thickness t_2



5.18 EDAX pattern and its SEM image of specimen of thickness t_3

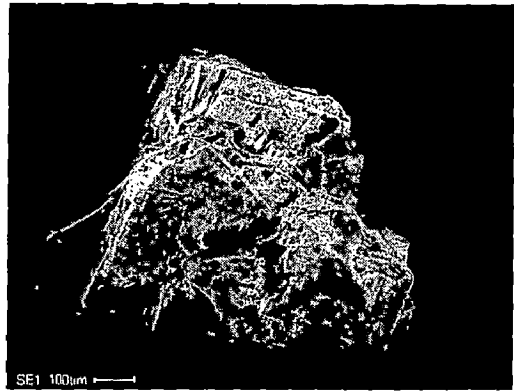
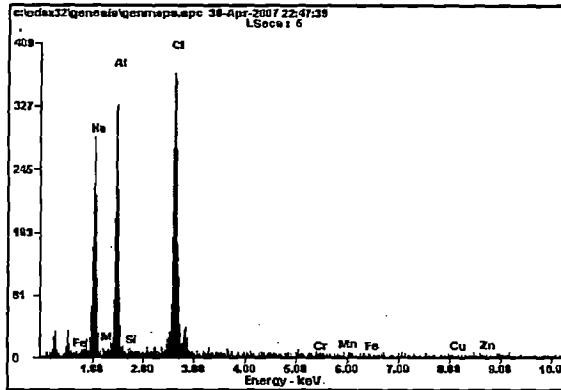


5.19 EDAX pattern and its SEM image of specimen of thickness t_4

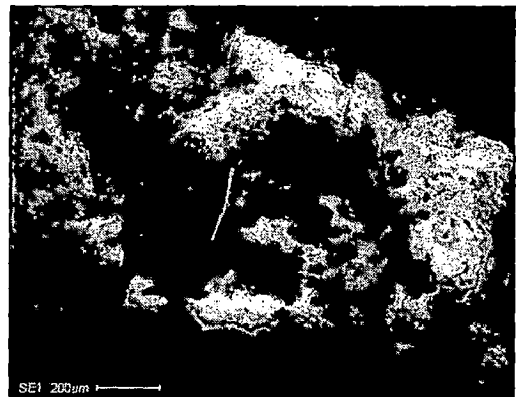
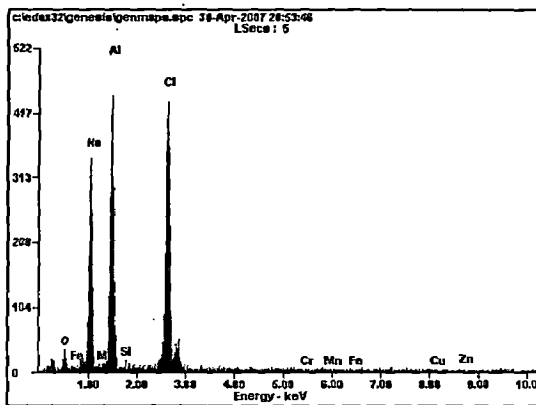


5.20 EDAX pattern and its SEM image of specimen of thickness t_5

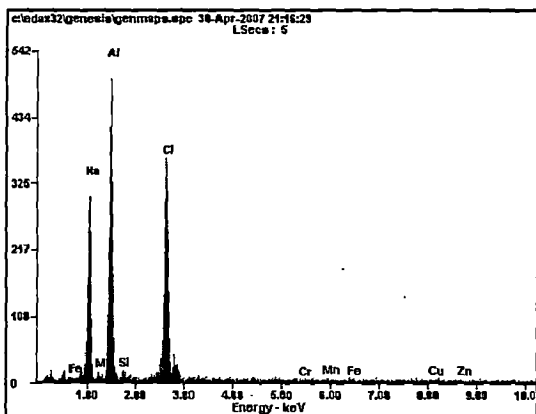
FESEM results for specimens undergo 48 hours duration test



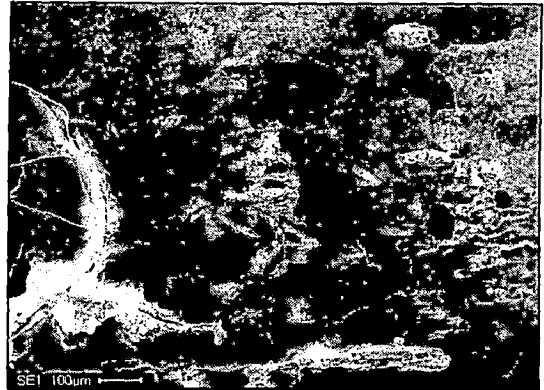
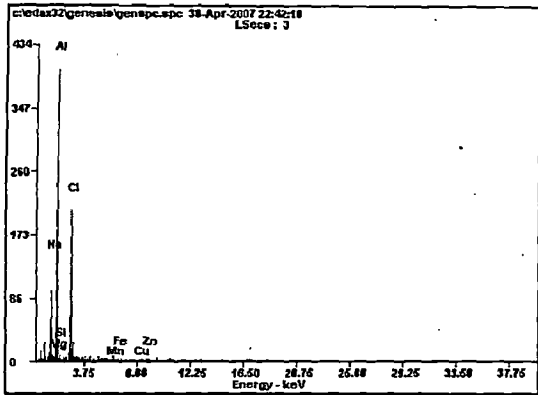
5.21 EDAX pattern and its SEM image of specimen of thickness t_1



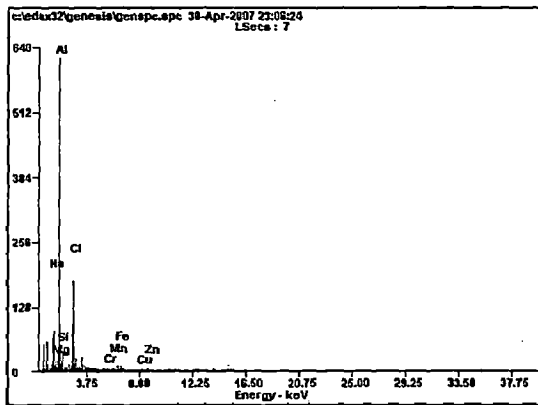
5.22 EDAX pattern and its SEM image of specimen of thickness t_2



5.23 EDAX pattern and its SEM image of specimen of thickness t_3

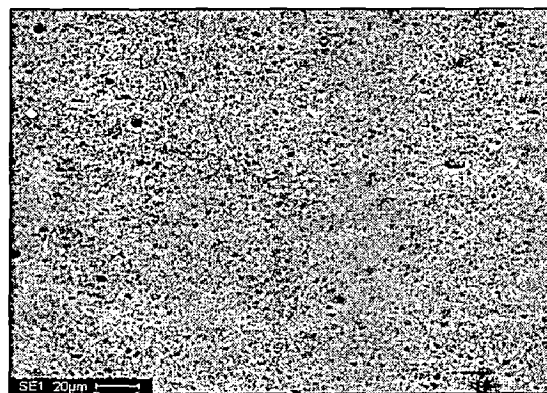
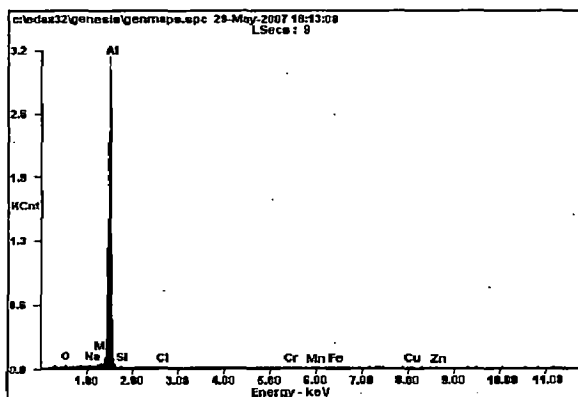


5.24 EDAX pattern and its SEM image of specimen of thickness t_4

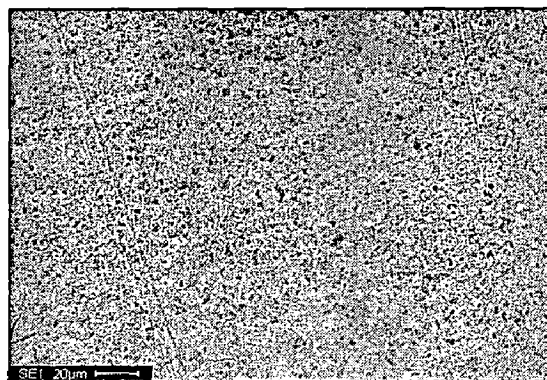
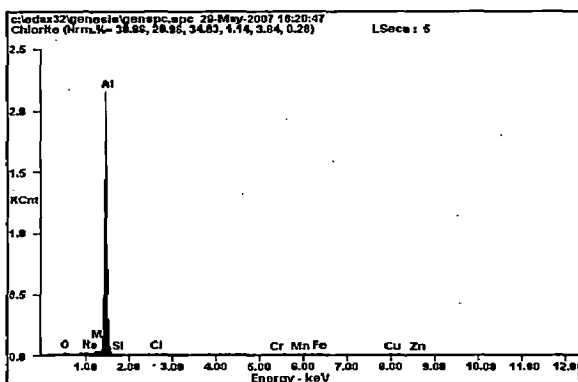


5.25 EDAX pattern and its SEM image of specimen of thickness t_5

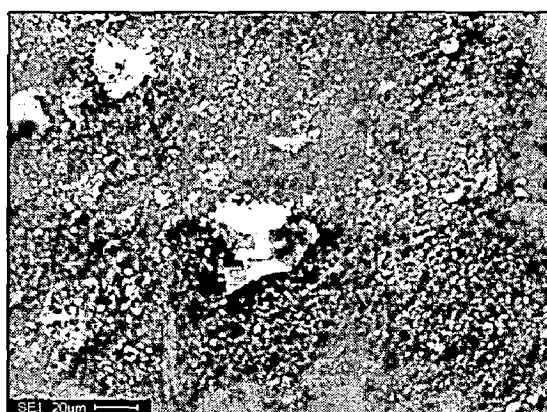
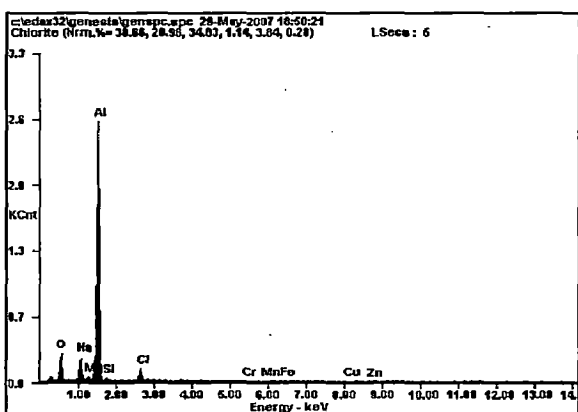
FESEM results for specimens undergo 72 hours duration test



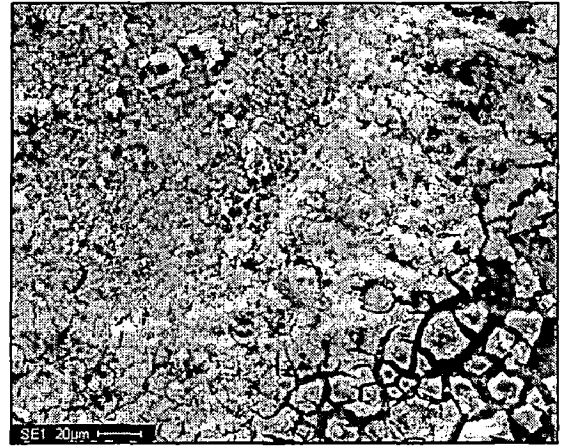
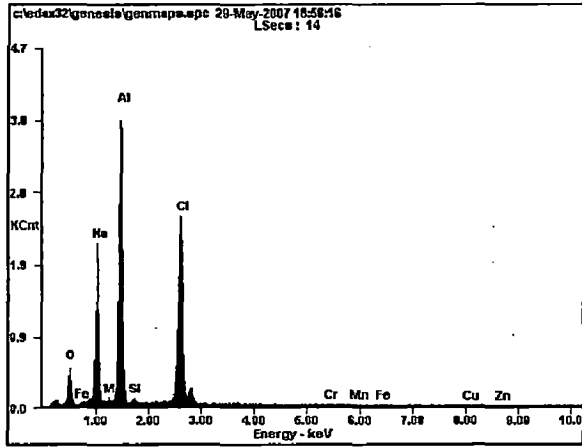
5.26 EDAX pattern and its SEM image of specimen of thickness t_1



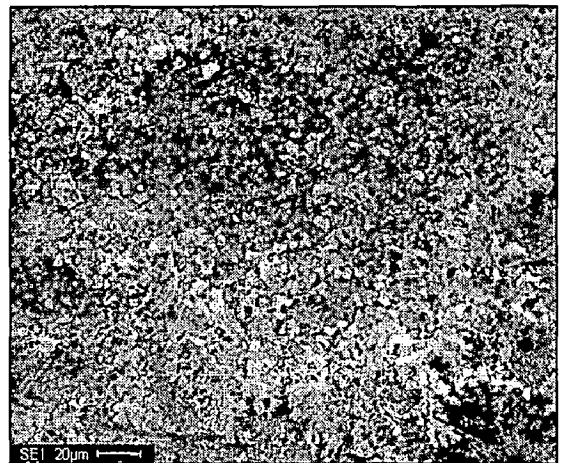
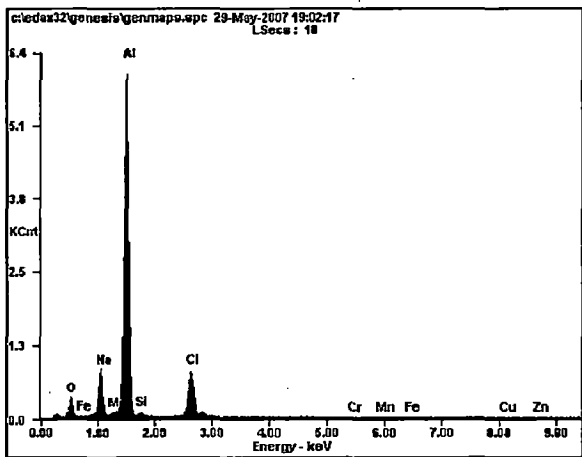
5.27 EDAX pattern and its SEM image of specimen of thickness t_2



5.28 EDAX pattern and its SEM image of specimen of thickness t_3



5.29 EDAX pattern and its SEM image of specimen of thickness t_4



5.30 EDAX pattern and its SEM image of specimen of thickness t_5

5.5 Discussions

All the nano-structured aluminium alloys processed by cryo-rolling in the present work have shown localized type of corrosion in 3.5% NaCl environment. Based on the thermo gravimetric data larger thickness specimen shown greater corrosion resistant as compared to minimum thickness specimen. As the duration of test increases minimum thickness specimen corrosion rate decreases and weight loss also diminished this shows that passivation behavior of material after certain period of time.

The XRD revealed the presence of Cr_2O_3 , Al_2O_3 , CuAl_2O_3 , $\text{FeO} \cdot \text{Cr}_2\text{O}_3$, $\text{Na}_2\text{SiO}_3 \cdot 9\text{H}_2\text{O}$, $\text{Cr}_2\text{O}_3 \cdot \text{FeO}$, $\text{Zn}(\text{AlO}_2)_2$, $\text{Mg}(\text{ClO}_4)_2 \cdot 6\text{H}_2\text{O}$, and CuO in corroded specimen which is in well agreement with FESEM data. From the thermo gravimetric data it is revealed that as the duration test increases corrosion rate decreases but for the same duration test larger thickness material undergo less corrosion as compared to smaller thickness material. In all above discussed material aluminum oxide are the dominant phases. So larger thickness nano-structured aluminium alloys processed by cryo-rolling have better corrosion resistant as compared to lower thickness nano-structured aluminium alloys processed by cryo-rolling. Some of complex phases are shown by XRD results due to complex nature of aluminium alloys.

1. All different thickness nanostructured aluminium alloys processed by cryo-rolling have shown localized type of corrosion behavior.
2. As compared to smaller thickness nanostructured aluminium alloys processed by cryo-rolling larger thickness specimen have shown better corrosion resistance.
3. After long duration of exposure to salt environment corrosion rate decrease which shown that there has been passivation effect.
4. Both immersion and salt spray test shown that slight weight loss of nanostructured aluminium alloys processed by cryo-rolling.
5. From this study of corrosion behavior of nanostructured aluminium alloys processed by cryo-rolling in a 3.5% NaCl solution, it can be concluded that, in function of the conditions of treatment, this nanostructured aluminium alloys processed by cryo-rolling undergoes two type of localized corrosion process, leading to the formation of hemispherical and crystallographic pits. In agreement with the results obtained when nanostructured aluminium alloys processed by cryo-rolling corrodes freely in a solution of NaCl at 3.55 the samples undergo a process of corrosion localized to the area surrounding the precipitates of Al(Mn, Fe, Cr), which results in hemispherical pits.
6. From this study of corrosion behavior of nanostructured aluminium alloys processed by cryo-rolling in a 3.5% NaCl solution, it can be concluded that, in function of the conditions of treatment, this nanostructured aluminium alloys processed by cryo-rolling undergoes two type of localized corrosion process, leading to the formation of hemispherical and crystallographic pits. In agreement with the results obtained when nanostructured aluminium alloys processed by cryo-rolling corrodes freely in a solution of NaCl at 3.55 the samples undergo a process of corrosion localized to the area surrounding the precipitates of Al(Mn, Fe, Cr), which results in hemispherical pits.
7. The corrosion behaviour of nanostructured Al alloys processed by cryo-rolling qualitatively changes after cryo-rolling. Cryo processed samples shown high dissolution rate.

On the basis of the present study, further work is proposed in the following lines:

- To study the general and localized corrosion behavior of ultrafine/nano grained aluminium alloys by electrochemical techniques such as potentiostat and impedance spectroscopy.
- To investigate the effect of alloying elements and impurities on the corrosion behavior of ultrafine/nano grained Al alloys.

REFERENCES

- [1] R.Z. Valiev (Ed.), *Ann. Chim. Sci. Materiaux* 21 (1996) 369 (Special issue).
- [2] R.Z. Valiev, A.V. Korznikov, R.R. Mulyukov, *Mater. Sci. Eng. A* 168 (1993) 141.
- [3] R.Z. Valiev, I.V. Alexandrov, R.K. Islamgaliev, in: G.M. Chow, N.I. Noskova (Eds.), *Nanocrystalline Materials: Science and Technology*, Nato ASI, Kluwer Academic Publishers, Dordrecht, 1998, p. 121.
- [4] N. Tsuji, Y. Ito, Y. Saito, Y. Minamono, *Scripta Mater.* 47 (2002) 893.
- [5] Y. Saito, H. Utsunomiya, T. Sakai, *Acta Mater.* 47 (1999) 579.
- [6] R.Z. Valiev, R.K. Islamgaliev, I.V. Alexandrov, *Prog. Mater. Sci.* 45 (2000) 103.
- [7] Z.Y. Liu, L.X. Hu, E.D. Wang, *Mater. Sci. Eng. A* 255 (1998) 16.
- [8] M. Richert, Q. Liu, N. Hansen, *Mater. Sci. Eng. A* 260 (1999) 275.
- [9] Y. Wang, M. Chen, F. Zhou, E. Ma, *Nature* 419 (2002) 912.
- [10] R.Z. Valiev, E.V. Kozlov, F. Yu, F. Ivanov, J. Lian, A.A. Nazarov, B. Baudalet, *Acta Metall.* 42 (1994) 2467.
- [11] V.Y. Gertsman, M. Hoffmann, H. Gleiter, R. Birringer, *Acta Metall.* 42 (1994) 3539.
- [12] O.V. Mishin, V.Y. Gertsman, R.Z. Valiev, G. Gottstein, *Scripta Mater.* 35 (1996) 873.
- [13] N.A. Akhmadeev, N.P. Kobelev, R.R. Mulyukov, Ya.M. Soifer, R.Z. Valiev, *Acta Metall.* 41 (1993) 1041.
- [14] J. Lian, R.Z. Valiev, B. Baudalet, *Acta Metall.* 43 (1995) 4165.
- [15] S.R. Agnew, J.R. Weertman, *Mater. Sci. Eng. A* 244 (1998) 145.
- [16] J.R. Davis, *Corrosion of Aluminium and Aluminium Alloys*, ASM International, 1999.
- [17] W. Zeiger, M. Schneider, D. Scharnweber, H. Worch, *Corrosion behaviour of a nanocrystalline FeAl₈ alloy*, *Nanostructure. Mater.* 6 (1995) 1013.
- [18] X.Y. Wang, D.Y. Li, *Mechanical and electrochemical behavior of nanocrystalline surface of 304 stainless steel*, *Electrochim. Acta* 47 (2002) 3939.
- [19] S.J. Thorpe, B. Ramaswami, K.T. Aust, *Corrosion and Auger studies of a nickel-base metal-metalloid*, *J. Electrochem. Soc* 135 (1988) 2162.

- [20] A. Barbucci, G. Farne`, P. Matteazzi, R. Riccieri, G. Cerisola, Corrosion behaviour of nanocrystalline Cu₉₀Ni₁₀ alloy in neutral solution containing chlorides, *Corros. Sci* 41 (1999) 463.
- [21] Y. Li, F.H. Wang, G. Liu, Grain size effect on the electrochemical corrosion behaviour of surface nanocrystallized low-carbon steel, *Corrosion* 60 (2004) 891–896.
- [22] R. Rofagha, R. langer, A.M. El-Sherik, U. Erb, G. Palumbo, A.K. Aust, The corrosion behaviour of nanocrystalline nickel, *Scripta Metall. Mater.* 25 (1991) 2867.
- [23] Kh.M.S. Youssef, C.C. Koch, P.S. Fedkiw, Improved corrosion behavior of nanocrystalline zinc produced by pulse-current electro deposition, *Corros. Sci* 46 (2004) 51.
- [24] J. Zhao, L. Xia, A. Sehgal, D. Lu, R.L. McCreery, G.S. Frankel, Effects of chromate and chromate conversion coatings on corrosion of aluminum alloy 2024-T3, *Surf. Coat. Technol.* 140 (2001) 51–57.
- [25] L. Xia, E. Akiyama, G. Frankel, R. McCreery, Storage and release of soluble hexavalent chromium from chromate conversion coatings. Equilibrium aspects of Cr^{VI} concentration, *J. Electrochem. Soc.* 147 (2000) 2556.
- [26] J. Zhao, G. Frankel, R.L. McCreery, Corrosion protection of untreated AA-2024-T3 in chloride solution by a chromate conversion coating monitored with Raman spectroscopy, *J. Electrochem. Soc.* 145 (1998) 2258.
- [27] M.W. Kendig, A.J. Davenport, H.S. Isaacs, The mechanism of corrosion inhibition by chromate conversion coatings from X-ray absorption near edge spectroscopy (XANES), *Corros. Sci.* 34 (1993) 41–49.
- [28] F.W. Lytle, R.B. Greigor, G.L. Bibbins, K.Y. Blohowiak, R.E. Smith, G.D. Tuss, An investigation of the structure and chemistry of a chromium-conversion surface layer on aluminum, *Corros. Sci.* 37 (1995) 349–369.
- [29] M. Bethencourt, F.J. Botana, M.A. Cauqui, M. Marcos, M.A. Rodr y'guez, J.M. Rodr y'guez Izquierdo, Protection against corrosion in marine environments of AA5083 Al–Mg alloy by lanthanide chlorides, *J. Alloy. Compd.* 250 (1997) 455–460.
- [30] D.R. Arnott, B.R.W. Hinton, N.E. Ryan, Cerium conversion coatings for the corrosion protection of aluminum, *Mater. Perform.* 26 (1987) 42–47.

- [31] B. Davo', J.J. de Damborenea, Use of rare earth salts as electrochemical corrosion inhibitors for an Al–Li–Cu (8090) alloy in 3.56% NaCl, *Electrochim. Acta* 49 (2004) 4957–4965.
- [32] W. Neil, C. Garrard, The corrosion behaviour of aluminium–silicon carbide composites in aerated 3.5% sodium chloride, *Corros. Sci.* 36 (1994) 837–851.
- [33] A.J. Aldykewicz, H.S. Isaacs, A.J. Davenport, Investigation of cerium as a cathodic inhibitor for aluminum–copper alloys, *J. Electrochem. Soc.* 142 (1995) 3342.
- [34] A. Aballe, M. Bethencourt, F.J. Botana, M. Marcos, CeCl₃ and LaCl₃ binary solution as environment friendly corrosion inhibitors of AA5083 Al–Mg alloy in NaCl solutions, *J. Alloy. Compd.* 323–324 (2001) 855–858.
- [35] M. Bethencourt, F.J. Botana, M.J. Cano, M. Marcos, High protective, environmental friendly and shorttime developed conversion coatings for aluminium alloys, *Appl. Surf. Sci.* 189 (2002) 162–173.
- [36] G.M. Treacy, G.D. Wilcox, M.O.W. Richardson, *Surf. Coat. Technol.* 114 (1999) 260–268.

